Theory of rigidity and numerical analysis of density of states of two-dimensional amorphous solids with dispersed frictional grains in the linear response regime

AUTHOR(S):

Ishima, Daisuke; Saitoh, Kuniyasu; Otsuki, Michio; Hayakawa, Hisao

CITATION:

Ishima, Daisuke ...[et al]. Theory of rigidity and numerical analysis of density of states of two-dimensional amorphous solids with dispersed frictional grains in the linear response regime. Physical Review E 2023, 107(5): 054902.

ISSUE DATE:

2023-05

URL:

http://hdl.handle.net/2433/284928

PHYSICAL REVIEW E **107**, 054902 (2023)

Theory of rigidity and numerical analysis of density of states of two-dimensional amorphous solids with dispersed frictional grains in the linear response regime

Daisuke Ishima,[1,*] Kuniyasu Saitoh,[2] Michio Otsuki,[3] and Hisao Hayakawa[1]
[1]*Yukawa Institute for Theoretical Physics, Kyoto University, Kitashirakawa-oiwake cho, Sakyo-ku, Kyoto 606-8502, Japan*
[2]*Department of Physics, Faculty of Science, Kyoto Sangyo University, Motoyama, Kamigamo, Kita-ku, Kyoto 603-8555, Japan*
[3]*Graduate School of Engineering Science, Osaka University, Toyonaka, Osaka 560-8531, Japan*

(Received 13 July 2022; accepted 23 March 2023; published 10 May 2023)

Using the Jacobian matrix, we obtain a theoretical expression of rigidity and the density of states of two-dimensional amorphous solids consisting of frictional grains in the linear response to an infinitesimal strain, in which we ignore the dynamical friction caused by the slip processes of contact points. The theoretical rigidity agrees with that obtained by molecular dynamics simulations. We confirm that the rigidity is smoothly connected to the value in the frictionless limit. We find that there are two modes in the density of states for sufficiently small k_T/k_N, which is the ratio of the tangential to normal stiffness. Rotational modes exist at low frequencies or small eigenvalues, whereas translational modes exist at high frequencies or large eigenvalues. The location of the rotational band shifts to the high-frequency region with an increase in k_T/k_N and becomes indistinguishable from the translational band for large k_T/k_N.

DOI: 10.1103/PhysRevE.107.054902

I. INTRODUCTION

Amorphous materials consisting of dispersed grains such as powders, colloids, bubbles, and emulsions are ubiquitous in nature [1–4]. These materials behave like liquids at low densities and exhibit solidlike mechanical responses above their jamming point [5]. In systems consisting of frictionless grains, the rigidity changes continuously, but the coordination number of grains changes discontinuously at the jamming point as a function of density [2,3,6]. The critical behavior near the jamming point is of interest to physicists as a nonequilibrium phase transition [7–11]. Dispersed grains above the jamming point are fragile and exhibit softening and yielding transition under certain loads [12–21].

For amorphous solids consisting of frictionless grains, it is useful to analyze the dynamical matrix or the Hessian matrix, which is defined as the second derivative of the potential of a collection of grains with respect to the displacements from their stable configuration [3,4,22–26]. For instance, the rigidity can be determined by eigenvalues and eigenvectors [27–32]. It has been reported that the minimum nonzero eigenvalue of the Hessian matrix decreases with increasing strain and eventually becomes negative, where an irreversible stress drop takes place [29,30,33–35].

It has long been known that amorphous solids have characteristic properties at low temperatures (e.g., thermal conductivity and specific heat) that are quite different from those of crystalline solids [36]. These days, we have recognized that amorphous solids consisting of dispersed grains exhibit unique elastic-plastic behavior as a mechanical response to an applied strain [37]. Because these properties are related to the density of states (DOS), there have been many studies on the DOS [6,24,38–40]. The DOSs for systems composed of anisotropic grains, such as ellipses, dimers, deformable grains, and grains with rough surfaces, have been studied with the aid of the Hessian matrix [41–51]. Because of the rotation of such anisotropic grains, there exists a rotational band in the DOS that is distinguishable from the translational band [42,44,45,48,50,51].

Even for systems of spherical grains that cannot be free from interparticle friction, similar results are expected as a result of grain rotations. However, few studies have reported the existence of rotational bands in the DOS. Because the frictional force between the grains depends on the contact history, it cannot be expressed as a conservative force. Therefore, stability analysis for frictional grains based on the Hessian cannot be used. Nevertheless, the Hessian analysis using an effective potential for frictional grains has been performed [52,53]. Recently, Liu *et al.* suggested that the Hessian analysis with another effective potential can be used even if slip processes exist [54]. Previous studies [52,53] reported that friction between grains causes a continuous change in the functional form of the DOS from that of frictionless systems. However, there are only a few reports on whether an isolated band in the DOS originating from friction between grains is visible at lower frequencies.

Recently, Chattoraj *et al.* discussed the stability of the grain configuration under strain using the Jacobian matrix of frictional grains [55]. They performed eigenvalue analysis under athermal quasistatic shear processes, and they determined the existence of oscillatory instability originating from interparticle friction at a certain strain [55–57]. However, they did not discuss the rigidity or the DOS.

*Present address: Simplex Holdings, Inc., 19F Toranomon Hills Mori Tower, 1-23-1 Toranomon, Minato-ku, Tokyo 105-6319, Japan; ishima.daisuke.m30@kyoto-u.ac.jp

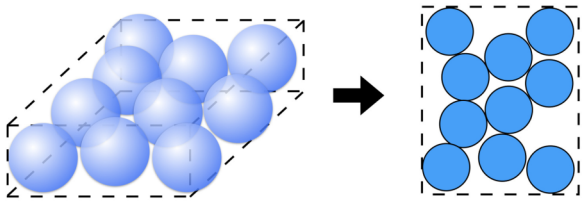

FIG. 1. Schematics of our system.

The theoretical determination of the rigidity of amorphous solids consisting of frictional grains is important for controlling amorphous solids. However, we do not know how to determine the rigidity from the Jacobian for the frictional grains.

The purpose of this study is to clarify the role of mutual friction between grains in terms of the rigidity and DOS. We focus on the response to an infinitesimal strain from a stable configuration of grains without any strain to obtain tangible results. In this study, we assume that there is no slip between grains because of an infinitesimal strain, and we then deal with friction as static friction.

The remainder of this paper is organized as follows. In the next section, we introduce the numerical method. In Sec. III, we introduce the Jacobian. Section IV consists of Sec IV A, which deals with the theoretical prediction of rigidity in the linear response regime, and Sec. IV B, which deals with the DOS. In the final section, we summarize the results of our study and discuss future work. In Appendix A, we summarize the method for preparing a stable grain configuration before applying shear. In Appendix B, we explain the implementation of the numerical integration method in the proposed system. In Appendix C, we summarize some properties of the Jacobian. In Appendix D, we present the explicit expressions of the Jacobian. In Appendix E, we investigate the effects of rattlers. In Appendix F, we write down the explicit results of the Jacobian. In Appendix G, we derive the theoretical prediction of rigidity using the Jacobian. In Appendix H, we introduce the DOS using the Hessian analysis. In Appendix I, we investigate the system size dependence of the DOS. In Appendix J, we study the density dependence of the DOS.

II. NUMERICAL MODEL

Our system contains N frictional spherical particles embedded in a monolayer configuration. We treat this system as a two-dimensional system (see Fig. 1). To prevent the system from crystallizing [58], we prepare an equal number of particles with diameters d and $d/1.4$. We assume that the mass of particle i is proportional to d_i^2, where d_i is the diameter of the ith particle. We introduce m as the mass of a particle with diameter d. In this study, x_i, y_i, and θ_i denote x, y coordinates and the rotational angle of the ith particle, respectively. We introduce the generalized coordinates of the ith particle $\boldsymbol{q}_i := (\boldsymbol{r}_i^{\mathrm{T}}, \ell_i)^{\mathrm{T}}$ with $\boldsymbol{q}_i := (x_i, y_i)^{\mathrm{T}}$ and $\ell_i := d_i\theta_i/2$, where the superscript T denotes the transposition.

Let the force and the z-component of the torque acting on the ith particle be $\boldsymbol{F}_i := (F_i^x, F_i^y)^{\mathrm{T}}$ and T_i, respectively. Then, the equations of motion of the ith particle are expressed as

$$m_i \frac{d^2\boldsymbol{r}_i}{dt^2} = \boldsymbol{F}_i, \tag{1}$$

$$I_i \frac{d^2\theta_i}{dt^2} = T_i \tag{2}$$

with the mass m_i and the momentum of inertia $I_i := m_i d_i^2/8$ of the ith particle. In a system without volume forces such as gravity, we can write

$$\boldsymbol{F}_i = \sum_{j\neq i} \boldsymbol{f}_{ij}, \tag{3}$$

$$T_i = \sum_{j\neq i} T_{ij}, \tag{4}$$

where $\boldsymbol{f}_{ij}$ and T_{ij} are the force and z-component of the torque acting on the ith particle from the jth particle, respectively. Here, T_{ij} is given by

$$T_{ij} = -\frac{d_i}{2}\left(n_{ij}^x f_{ij}^y - n_{ij}^y f_{ij}^x\right), \tag{5}$$

where we have introduced the normal unit vector between i and j particles as $\boldsymbol{n}_{ij} := \boldsymbol{r}_{ij}/|\boldsymbol{r}_{ij}| := (\boldsymbol{r}_i - \boldsymbol{r}_j)/|\boldsymbol{r}_i - \boldsymbol{r}_j|$. Here, n_{ij}^ζ and f_{ij}^ζ refer to ζ-components of $\boldsymbol{n}_{ij}$ and $\boldsymbol{f}_{ij}$, respectively. Note that ζ expresses $\zeta = x$ or y throughout this study. The force $\boldsymbol{f}_{ij}$ can be divided into normal $\boldsymbol{f}_{N,ij}$ and tangential $\boldsymbol{f}_{T,ij}$ parts as

$$\boldsymbol{f}_{ij} = (\boldsymbol{f}_{N,ij} + \boldsymbol{f}_{T,ij})\Theta(d_{ij}/2 - |\boldsymbol{r}_{ij}|), \tag{6}$$

where $d_{ij} := d_i + d_j$, and $\Theta(x)$ is the Heaviside step function, taking $\Theta(x) = 1$ for $x > 0$ and $\Theta(x) = 0$ otherwise. We model the repulsive force between the contacted particles i and j as the Hertzian force in addition to the dissipative force proportional to the relative velocity with a damping constant η_D [54] as follows:

$$\boldsymbol{f}_{N,ij} := k_N \xi_{N,ij}^{3/2} \boldsymbol{n}_{ij} - \eta_D \boldsymbol{v}_{N,ij}, \tag{7}$$

$$\boldsymbol{f}_{T,ij} := k_T \xi_{N,ij}^{1/2} \xi_{T,ij} \boldsymbol{t}_{ij} - \eta_D \boldsymbol{v}_{T,ij}, \tag{8}$$

where k_N and k_T are the stiffness parameters of normal and tangential contacts, respectively. The normal compression length and its velocity are denoted as $\xi_{N,ij} := d_{ij}/2 - |\boldsymbol{r}_{ij}|$ and $\boldsymbol{v}_{N,ij} = (\dot{\boldsymbol{r}}_{ij} \cdot \boldsymbol{n}_{ij})\boldsymbol{n}_{ij}$, respectively. For the tangential deformation, with the aid of $\boldsymbol{u}_{ij} := (n_{ij}^y, -n_{ij}^x)^{\mathrm{T}}$, the tangential velocity $\boldsymbol{v}_{T,ij}$ is defined as $\boldsymbol{v}_{T,ij} := \dot{\boldsymbol{r}}_{ij} - \boldsymbol{v}_{N,ij} + \boldsymbol{u}_{ij}(d_i\omega_i + d_j\omega_j)/2$, where we have introduced

$$\boldsymbol{\xi}_{T,ij} := \int_{C_{ij}} dt\, \boldsymbol{v}_{T,ij} - \left[\left(\int_{C_{ij}} dt\, \boldsymbol{v}_{T,ij}\right) \cdot \boldsymbol{n}_{ij}\right] \boldsymbol{n}_{ij}, \tag{9}$$

with $\xi_{T,ij} := |\boldsymbol{\xi}_{T,ij}|$ and $\boldsymbol{t}_{ij} := -\boldsymbol{\xi}_{T,ij}/\xi_{T,ij}$. Here, $\dot{\boldsymbol{A}} := d\boldsymbol{A}/dt$, and $\int_{C_{ij}} dt$ is the integration over the duration time of contact between i and j particles. Although the dissipative force between grains interacting with the Hertzian force is proportional to the product of the relative velocity and $\xi_{N,ij}^{1/2}$ [59–61], we adopt simple dissipative forces as in Eqs. (7) and (8) because we are not interested in the relaxation dynamics. We note that Eqs. (7) and (8) assume the Hertzian contact force for the static repulsion of contacting spheres, but all calculations in this study are those for two-dimensional systems. Here, we do not consider the effects of slips in the tangential equation of motion. This treatment can be justified if we restrict our interest in the linear response regime to

a stable configuration of particles without any strain. This situation corresponds to frictional grains with an infinitely large dynamical friction constant, in which the friction is only characterized by static friction. Therefore, our analysis does not apply to systems with finite strain [62], where the effect of slip is important.

To generate a stable configuration of frictional particles, we prepare a stable configuration of frictionless particles in a square box of linear size L using a fast inertial relaxation engine (FIRE) [63]. Subsequently, we turn on the tangential force using Eqs. (1) and (2) to achieve a stable configuration in the force-balanced (FB) state for frictional particle[1] (see Appendix A for details). Here, the FB state satisfies the FB conditions $|F_i^\zeta| = 0$ and $|T_i| = 0$ for arbitrary particles. Note that we set $\theta_i = 0$ when the tangential force is turned on.

We impose the Lees-Edwards boundary condition [64,65], where the direction parallel to the shear strain is the x-direction. After applying a step strain $\Delta\gamma$ to all particles, the x-coordinate of the position of the ith particle is shifted by an affine displacement $\Delta x_i(\Delta\gamma) := \Delta\gamma y_i^{\mathrm{FB}}(0)$, where the superscript FB denotes the FB state. The system is then relaxed to the FB state by the contact forces between the particles expressed in Eqs. (7) and (8). Here, ζ-components of translational $\Delta\mathring{r}_i^\zeta(\Delta\gamma)$ and rotational $\Delta\mathring{\ell}_i(\Delta\gamma)$ nonaffine displacements of the ith particle after the relaxation process are, respectively, defined as

$$\Delta\mathring{r}_i^\zeta(\Delta\gamma) := r_i^{\mathrm{FB},\zeta}(\Delta\gamma) - r_i^{\mathrm{FB},\zeta}(0) - \delta_{\zeta x}\Delta\gamma y_i^{\mathrm{FB}}(0), \quad (10)$$

$$\Delta\mathring{\ell}_i := \ell_i^{\mathrm{FB}}(\Delta\gamma) - \ell_i^{\mathrm{FB}}(0). \quad (11)$$

Using Eqs. (10) and (11), we introduce the rate of nonaffine displacements as

$$\frac{d\mathring{r}_i^\zeta}{d\gamma} := \lim_{\Delta\gamma\to 0}\frac{\Delta\mathring{r}_i^\zeta(\Delta\gamma)}{\Delta\gamma} = \lim_{\Delta\gamma\to 0}\frac{r_i^{\mathrm{FB},\zeta}(\Delta\gamma) - r_i^{\mathrm{FB},\zeta}(0)}{\Delta\gamma} - \delta_{\zeta x}y_i^{\mathrm{FB}}(0), \quad (12)$$

$$\frac{d\mathring{\ell}_i}{d\gamma} := \lim_{\Delta\gamma\to 0}\frac{\Delta\mathring{\ell}_i(\Delta\gamma)}{\Delta\gamma} = \lim_{\Delta\gamma\to 0}\frac{\ell_i^{\mathrm{FB}}(\Delta\gamma) - \ell_i^{\mathrm{FB}}(0)}{\Delta\gamma}. \quad (13)$$

Our system is characterized by the generalized coordinate $\boldsymbol{q}(\gamma) := (\boldsymbol{q}_1^{\mathrm{T}}(\gamma), \boldsymbol{q}_2^{\mathrm{T}}(\gamma), \ldots, \boldsymbol{q}_N^{\mathrm{T}}(\gamma))^{\mathrm{T}}$. The configuration in the FB state at strain γ is denoted as $\boldsymbol{q}^{\mathrm{FB}}(\gamma) := ((\boldsymbol{q}_1^{\mathrm{FB}}(\gamma))^{\mathrm{T}}, (\boldsymbol{q}_2^{\mathrm{FB}}(\gamma))^{\mathrm{T}}, \ldots, (\boldsymbol{q}_N^{\mathrm{FB}}(\gamma))^{\mathrm{T}})^{\mathrm{T}}$. The shear stress $\sigma_{xy}(\gamma)$ at $\boldsymbol{q}^{\mathrm{FB}}(\gamma)$ for one sample is given by

$$\sigma_{xy}(\boldsymbol{q}^{\mathrm{FB}}(\gamma)) = -\frac{1}{L^2}\sum_i\sum_{j>i} f_{ij}^x(\boldsymbol{q}^{\mathrm{FB}}(\gamma))r_{ij}^y(\boldsymbol{q}^{\mathrm{FB}}(\gamma)). \quad (14)$$

The rigidity g in the linear response regime for one sample is defined as

$$g := \left.\frac{d\sigma_{xy}(\boldsymbol{q}(\gamma))}{d\gamma}\right|_{\boldsymbol{q}(\gamma)=\boldsymbol{q}^{\mathrm{FB}}(0)}, \quad (15)$$

where the differentiation on the right-hand side (RHS) of Eq. (15) is defined as follows:

$$\left.\frac{d\sigma_{xy}(\boldsymbol{q}(\gamma))}{d\gamma}\right|_{\boldsymbol{q}(\gamma)=\boldsymbol{q}^{\mathrm{FB}}(0)} := \lim_{\Delta\gamma\to 0}\frac{\sigma_{xy}(\boldsymbol{q}^{\mathrm{FB}}(\Delta\gamma)) - \sigma_{xy}(\boldsymbol{q}^{\mathrm{FB}}(0))}{\Delta\gamma}. \quad (16)$$

In the numerical calculation, we use a nonzero but sufficiently small $\Delta\gamma$ for the evaluation of g. Then, the rigidity G in the linear response regime is defined as

$$G := \langle g\rangle, \quad (17)$$

where $\langle\cdot\rangle$ is the ensemble average.

For the numerical FB condition, we use the condition $|\tilde{F}_i^\alpha| < F_{\mathrm{Th}}$ for arbitrary i, where F_{Th} is the threshold force for the simulation, and $\tilde{\boldsymbol{F}}_i$ is the generalized force, defined as $\tilde{\boldsymbol{F}}_i := (\tilde{F}_i^x, \tilde{F}_i^y, \tilde{F}_i^\ell)^{\mathrm{T}} := (F_i^x, F_i^y, 2T_i/d_i)^{\mathrm{T}}$.

In our simulation, we adopt $\eta_D = (mk_N)^{1/2}d^{1/4}$ and $F_{\mathrm{Th}} = 1.0\times 10^{-14}k_N d^{3/2}$. The control parameters are the ratio of the tangential to normal stiffness k_T/k_N and projected area fraction to two-dimensional space ϕ. The operating ranges of k_T/k_N and ϕ are 0.0–10.0 and 0.83–0.90, respectively. In this study, we mainly present the results for $N = 4096$ and $\Delta\gamma = 1.0\times 10^{-6}$ with the ensemble averages of 10 samples for each k_T/k_N and ϕ. Some results are obtained with $N = 1024$, $\Delta\gamma = 1.0\times 10^{-6}$, and five samples for each k_T/k_N and ϕ. We verify that the results are independent of the choice of $\Delta\gamma$ for $1.0\times 10^{-6} \leqslant \Delta\gamma \leqslant 1.0\times 10^{-4}$. We ignore the effect of dissipation between particles because the velocity of each particle is sufficiently small for infinitesimal agitation from the FB state. The time step of the simulation, Δt, was set to $\Delta t = 1.0\times 10^{-2}t_0$, and numerical integration was performed using the velocity Verlet method (see Appendix B), where $t_0 := (m/k_N)^{1/2}d^{1/4}$. To obtain eigenvalues and eigenvectors of the Jacobian matrix, which will be introduced in detail in the next section, we have used the LAPACK, which provides a template library for linear algebra.

[1]For simplicity, we prepare the configuration before applying shear for frictionless particles at first, and then we consider the friction between particles. If we prepare a configuration before applying shear by compressing frictional particles, we confirm that the configuration had an oscillatory instability that resulted from the appearance of a pair of imaginary eigenvalues of the Jacobian divided by the mass matrix: $\lambda' = \lambda_r' \pm i\lambda_i'$ [55–57], where λ', λ_r', and λ_i' are the complex, real, and imaginary eigenvalues of $M^{-1}\mathcal{J}$, respectively. Here, $\mathcal{J}$ is the Jacobian defined in Eq. (18), and M is the mass matrix whose explicit form is given by $M = \begin{bmatrix} M_1 & & \\ & \ddots & \\ & & M_N \end{bmatrix}$, where $M_i := \begin{bmatrix} m_i & & \\ & m_i & \\ & & 4I_i/d_i^2 \end{bmatrix}$. Because the linearized equation of motion is expressed as $d^2q_i^\alpha/dt^2 = -\sum_{k,\kappa}\sum_{j,\beta}(M_{ik}^{\alpha\kappa})^{-1}\mathcal{J}_{kj}^{\kappa\beta}q_j^\beta$, there are four fundamental solutions $\boldsymbol{q} \propto e^{i\omega_n' t}$, where $i\omega_n'$ consists of $i\omega_{\pm 1}' = \omega_i' \pm i\omega_r'$ and $i\omega_{\pm 2}' = -\omega_i' \pm i\omega_r'$. Here, ω_r' and ω_i' satisfy the relation $\omega_r' \pm i\omega_i' = \sqrt{\lambda_r' \pm i\lambda_i'}$. Thus, to avoid the oscillatory instability of the configuration before applying shear, we adopt the protocol of creating the configuration with frictionless particles, and then let the system relax by adding static friction between particles.

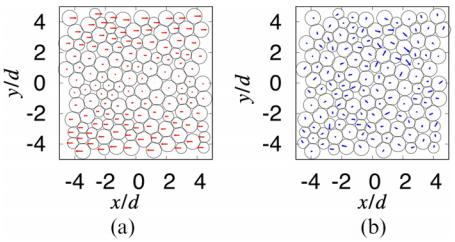

FIG. 2. Plots of (a) affine displacements and (b) nonaffine displacements of particles with $\Delta\gamma = 1.0 \times 10^{-6}$. Here, the magnitudes of the vectors are multiplied by (a) $0.1\Delta\gamma^{-1}$ and (b) 1.3 for the visualization. These figures are based on numerical results for $N = 128$.

Figure 2(a) shows an example of the affine displacements of particles, where the displacements exist only in the shear direction, and Fig. 2(b) shows the nonaffine displacements.

III. THEORETICAL ANALYSIS

In this section, we introduce the Jacobian, the DOS, and theoretical expressions of the linear rigidity. Here, we omit the effects of $\dot{\boldsymbol{q}}$ because the dissipative term proportional to $\dot{\boldsymbol{q}}$ vanishes under quasistatic shear.

A. Jacobian and the DOS for frictional particles

In frictional systems, the stability of the system and DOS at $\boldsymbol{q}^{\rm FB}(\gamma)$ are analyzed using the Jacobian ($\mathcal{J}$) defined as [55]

$$\mathcal{J}_{ij}^{\alpha\beta} := -\left.\frac{\partial \tilde{F}_i^{\alpha}(\boldsymbol{q}(\gamma))}{\partial q_j^{\beta}}\right|_{\boldsymbol{q}(\gamma)=\boldsymbol{q}^{\rm FB}(0)}, \tag{18}$$

where α and β are any of x, y, and ℓ, while i and j express particle indices. Therefore, the Jacobian matrix, which is a $3N \times 3N$ matrix, can be written as

$$\mathcal{J} = \begin{bmatrix} \mathcal{J}_{11} & \cdots & \mathcal{J}_{1i} & \cdots & \mathcal{J}_{1j} & \cdots & \mathcal{J}_{1N} \\ \vdots & \ddots & \vdots & & \vdots & & \vdots \\ \mathcal{J}_{i1} & \cdots & \mathcal{J}_{ii} & \cdots & \mathcal{J}_{ij} & \cdots & \mathcal{J}_{iN} \\ \vdots & & \vdots & \ddots & \vdots & & \vdots \\ \mathcal{J}_{j1} & \cdots & \mathcal{J}_{ji} & \cdots & \mathcal{J}_{jj} & \cdots & \mathcal{J}_{jN} \\ \vdots & & \vdots & & \vdots & \ddots & \vdots \\ \mathcal{J}_{N1} & \cdots & \mathcal{J}_{Ni} & \cdots & \mathcal{J}_{Nj} & \cdots & \mathcal{J}_{NN} \end{bmatrix}, \tag{19}$$

where $\mathcal{J}_{ij}$ is a 3×3 submatrix of the Jacobian $\mathcal{J}$ for a pair of particles i and j:

$$\mathcal{J}_{ij} = \begin{bmatrix} \mathcal{J}_{ij}^{xx} & \mathcal{J}_{ij}^{xy} & \mathcal{J}_{ij}^{x\ell} \\ \mathcal{J}_{ij}^{yx} & \mathcal{J}_{ij}^{yy} & \mathcal{J}_{ij}^{y\ell} \\ \mathcal{J}_{ij}^{\ell x} & \mathcal{J}_{ij}^{\ell y} & \mathcal{J}_{ij}^{\ell\ell} \end{bmatrix}. \tag{20}$$

See Appendixes C and D for detailed properties of the Jacobian. The right and left eigenvalue equations of $\mathcal{J}$ are, respectively, given by

$$\mathcal{J}\,|R_n\rangle = \lambda_n\,|R_n\rangle\,, \tag{21}$$

$$\langle L_n|\,\mathcal{J} = \lambda_n\,\langle L_n|\,, \tag{22}$$

where $|R_n\rangle$ and $\langle L_n|$ are the right and left eigenvectors corresponding to λ_n, respectively. Here, λ_n is the nth eigenvalue of $\mathcal{J}$. Note that $|R_n\rangle$ and $\langle L_n|$ satisfy the orthonormal relation $\langle L_m|R_n\rangle = \delta_{mn}$ with normalization $\langle R_n|R_n\rangle = \langle L_n|L_n\rangle = 1$ if all eigenstates are nondegenerate. Here, the inner products for the right and left eigenvectors are defined as $\langle R_n|R_n\rangle = \sum_{i=1}^{N}\sum_{\alpha=x,y,\ell}|R_{n,i}^{\alpha}|^2$ and $\langle L_n|L_n\rangle = \sum_{i=1}^{N}\sum_{\alpha=x,y,\ell}|L_{n,i}^{\alpha}|^2$, respectively. In the presence of friction, the eigenvalue λ_n is generally a complex number, but if we restrict our interest to infinitesimal distortions from stable configurations without shear strain, λ_n becomes real and can be expressed as $\lambda_n = \omega_n^2$. The DOS is the distribution function of the eigenvalues, defined as

$$D(\omega) := \frac{1}{3N}\sum_{n}{}'\langle\delta(\omega-\omega_n)\rangle, \tag{23}$$

where $\sum_n'$ on the right-hand side (RHS) of Eq. (23) expresses that the summation excludes the contribution of rattlers (see Appendix E for the details on the rattlers). Using the force decomposition, the Jacobian can also be divided into

$$\mathcal{J}_{ij}^{\alpha\beta} = \mathcal{J}_{N,ij}^{\alpha\beta} + \mathcal{J}_{T,ij}^{\alpha\beta}, \tag{24}$$

where

$$\mathcal{J}_{N,ij}^{\alpha\beta} := \left.\frac{\partial \tilde{f}_{N,ij}^{\alpha}(\boldsymbol{q}(\gamma))}{\partial q_j^{\beta}}\right|_{\boldsymbol{q}(\gamma)=\boldsymbol{q}^{\rm FB}(\gamma)}, \tag{25}$$

$$\mathcal{J}_{T,ij}^{\alpha\beta} := \left.\frac{\partial \tilde{f}_{T,ij}^{\alpha}(\boldsymbol{q}(\gamma))}{\partial q_j^{\beta}}\right|_{\boldsymbol{q}(\gamma)=\boldsymbol{q}^{\rm FB}(\gamma)} \tag{26}$$

for $i \neq j$ and

$$\mathcal{J}_{N,ij}^{\alpha\beta} := \sum_{(i,k)}\left.\frac{\partial \tilde{f}_{N,ik}^{\alpha}(\boldsymbol{q}(\gamma))}{\partial q_i^{\beta}}\right|_{\boldsymbol{q}(\gamma)=\boldsymbol{q}^{\rm FB}(\gamma)}, \tag{27}$$

$$\mathcal{J}_{T,ij}^{\alpha\beta} := \sum_{(i,k)}\left.\frac{\partial \tilde{f}_{T,ik}^{\alpha}(\boldsymbol{q}(\gamma))}{\partial q_i^{\beta}}\right|_{\boldsymbol{q}(\gamma)=\boldsymbol{q}^{\rm FB}(\gamma)} \tag{28}$$

for $i = j$. Here, we have introduced $\tilde{\boldsymbol{f}}_{N,ij} = (\tilde{f}_{N,ij}^x, \tilde{f}_{N,ij}^y, \tilde{f}_{N,ij}^\ell)^{\rm T} = (f_{N,ij}^x, f_{N,ij}^y, 0)^{\rm T}$ and $\tilde{\boldsymbol{f}}_{T,ij} = (\tilde{f}_{T,ij}^x, \tilde{f}_{T,ij}^y, \tilde{f}_{T,ij}^\ell)^{\rm T} = (f_{T,ij}^x, f_{T,ij}^y, 2T_{ij}/d_i)^{\rm T}$, where $f_{N,ij}^{\zeta}$ and $f_{T,ij}^{\zeta}$ are ζ-components of $\boldsymbol{f}_{N,ij}$ and $\boldsymbol{f}_{T,ij}$, respectively. Note that $\sum_{(i,j)}$ denotes the summation for contacted particles of the ith particle. The explicit expressions of $\mathcal{J}_{N,ij}^{\alpha\beta}$ and $\mathcal{J}_{T,ij}^{\alpha\beta}$ are presented in Appendix F.

B. Expressions of the linear rigidity via eigenmodes

Let us introduce $|\tilde{F}(\boldsymbol{q}(\gamma))\rangle$ as

$$|\tilde{F}(\boldsymbol{q}(\gamma))\rangle := \left[\tilde{\boldsymbol{F}}_1^{\rm T}(\boldsymbol{q}(\gamma)), \tilde{\boldsymbol{F}}_2^{\rm T}(\boldsymbol{q}(\gamma)), \ldots, \tilde{\boldsymbol{F}}_N^{\rm T}(\boldsymbol{q}(\gamma))\right]^{\rm T}. \tag{29}$$

Because the forces acting on the particles are balanced in the FB state, $|\tilde{F}(\boldsymbol{q}(\gamma))\rangle\,|_{\boldsymbol{q}(\gamma)=\boldsymbol{q}^{\rm FB}(\gamma)}$ satisfies

$$|\tilde{F}(\boldsymbol{q}(\gamma))\rangle\,|_{\boldsymbol{q}(\gamma)=\boldsymbol{q}^{\rm FB}(\gamma)} = |0\rangle\,, \tag{30}$$

where $|0\rangle$ is the ket vector containing 0 for all components. The stable configuration in the FB state satisfies

$$\left.\frac{d\,|\tilde{F}(\boldsymbol{q}(\gamma))\rangle}{d\gamma}\right|_{\boldsymbol{q}(\gamma)=\boldsymbol{q}^{\rm FB}(0)} = |0\rangle\,, \tag{31}$$

where

$$\left.\frac{d\,|\tilde{F}(\boldsymbol{q}(\gamma))\rangle}{d\gamma}\right|_{\boldsymbol{q}(\gamma)=\boldsymbol{q}^{\mathrm{FB}}(0)} := \lim_{\Delta\gamma\to 0}\frac{|\tilde{F}(\boldsymbol{q}^{\mathrm{FB}}(\Delta\gamma))\rangle - |\tilde{F}(\boldsymbol{q}^{\mathrm{FB}}(0))\rangle}{\Delta\gamma}. \tag{32}$$

Introducing

$$\left|\frac{d\mathring{q}}{d\gamma}\right\rangle := \left[\frac{d\mathring{r}_1^x}{d\gamma}, \frac{d\mathring{r}_1^y}{d\gamma}, \frac{d\mathring{\ell}_1}{d\gamma}, \ldots, \frac{d\mathring{r}_N^x}{d\gamma}, \frac{d\mathring{r}_N^y}{d\gamma}, \frac{d\mathring{\ell}_N}{d\gamma}\right]^{\mathrm{T}}, \tag{33}$$

the left-hand side (LHS) of Eq. (31) can be rewritten as

$$\left.\frac{d\,|\tilde{F}(\boldsymbol{q}(\gamma))\rangle}{d\gamma}\right|_{\boldsymbol{q}(\gamma)=\boldsymbol{q}^{\mathrm{FB}}(0)} = -\,|\Xi\rangle + \tilde{\mathcal{J}}\left|\frac{d\mathring{q}}{d\gamma}\right\rangle, \tag{34}$$

where we have used Eqs. (12) and (13) (see Appendix G 1). The first and second terms on the RHS of Eq. (34) represent the strain derivatives of the forces for the contributions from the affine and nonaffine displacements, respectively. The explicit form of $|\Xi\rangle$ is given by

$$|\Xi\rangle := \begin{bmatrix} \sum_{j\neq 1}\mathcal{J}^{xx}_{N,j1}r^y_{1j} \\ \sum_{j\neq 1}\mathcal{J}^{xy}_{N,j1}r^y_{1j} \\ \sum_{j\neq 1}\mathcal{J}^{x\ell}_{N,j1}r^y_{1j} \\ \vdots \\ \sum_{j\neq N}\mathcal{J}^{xx}_{N,jN}r^y_{Nj} \\ \sum_{j\neq N}\mathcal{J}^{xy}_{N,jN}r^y_{Nj} \\ \sum_{j\neq N}\mathcal{J}^{x\ell}_{N,jN}r^y_{Nj} \end{bmatrix}. \tag{35}$$

Note that the tangential displacements do not contribute to $|\Xi\rangle$. This is because the affine displacements are applied to our system instantaneously as a step strain; thus, the integral interval of the tangential displacement during the affine deformation is zero. We have used $\tilde{\mathcal{J}}$ in Eq. (34) defined as

$$\tilde{\mathcal{J}}^{\alpha\beta}_{ii} := \begin{cases} -\mathcal{J}^{\ell x}_{ii} & (\alpha=\ell,\ \beta=x), \\ -\mathcal{J}^{\ell y}_{ii} & (\alpha=\ell,\ \beta=y), \\ \mathcal{J}^{\alpha\beta}_{ii} & (\text{otherwise}), \end{cases} \tag{36}$$

and

$$\tilde{\mathcal{J}}^{\alpha\beta}_{ij} := \begin{cases} -\mathcal{J}^{x\ell}_{ij} & (\alpha=x,\ \beta=\ell), \\ -\mathcal{J}^{y\ell}_{ij} & (\alpha=y,\ \beta=\ell), \\ \mathcal{J}^{\alpha\beta}_{ij} & (\text{otherwise}) \end{cases} \tag{37}$$

for $i\neq j$.

Expanding the nonaffine displacements by the eigenfunctions of $\tilde{\mathcal{J}}$ and using the fact that the LHS in Eq. (34) is zero, we obtain

$$\left|\frac{d\mathring{q}}{d\gamma}\right\rangle = {\sum_n}' \frac{\langle\tilde{L}_n|\Xi\rangle}{\tilde{\lambda}_n}\,|\tilde{R}_n\rangle\,, \tag{38}$$

where $\tilde{\lambda}_n$, $\langle\tilde{L}_n|$, and $|\tilde{R}_n\rangle$ are the nth eigenvalue of $\tilde{\mathcal{J}}$, and the left and right eigenvectors corresponding to $\tilde{\lambda}_n$, respectively. Note that $|\tilde{R}_n\rangle$ and $\langle\tilde{L}_n|$ satisfy the orthonormal relation $\langle\tilde{L}_m|\tilde{R}_n\rangle = \delta_{mn}$, if all eigenstates are nondegenerate. See Appendix G 1 for the derivation of Eq. (38).

The rigidity in the linear response regime under infinitesimal strain $\Delta\gamma$ is decomposed into two parts:

$$G := G_{\mathrm{A}} + G_{\mathrm{NA}}, \tag{39}$$

where G_{A} and G_{NA} are the rigidities corresponding to the affine and nonaffine displacements, respectively. With the aid of Eqs. (14), (17), and (37), the expressions of G_{A} and G_{NA} are, respectively, given by (see Appendix G 2)

$$G_{\mathrm{A}} := \frac{1}{2L^2}\left\langle \sum_{i,j(i\neq j)} \left(r^y_{ij}\right)^2 \mathcal{J}^{xx}_{N,ji} \right\rangle, \tag{40}$$

$$G_{\mathrm{NA}} := \frac{1}{2L^2}\left\langle \sum_{i,j(i\neq j)} \left[\sum_{\zeta=x,y} r^y_{ij}\tilde{\mathcal{J}}^{x\zeta}_{ij}\frac{d\mathring{r}^\zeta_{ij}}{d\gamma} - r^y_{ij}\tilde{\mathcal{J}}^{x\ell}_{ij}\frac{d\mathring{\ell}_{ij}}{d\gamma} \right] \right\rangle, \tag{41}$$

where we have introduced

$$\frac{d\mathring{r}^\zeta_{ij}}{d\gamma} := \frac{d\mathring{r}^\zeta_i}{d\gamma} - \frac{d\mathring{r}^\zeta_j}{d\gamma}, \tag{42}$$

$$\frac{d\mathring{\ell}_{ij}}{d\gamma} := \frac{d\mathring{\ell}_i}{d\gamma} + \frac{d\mathring{\ell}_j}{d\gamma}. \tag{43}$$

Substituting Eq. (38) into Eq. (41), G_{NA} can be rewritten as follows:

$$G_{\mathrm{NA}} = -\frac{1}{L^2}\left\langle {\sum_n}' \frac{\langle\tilde{L}_n|\Xi\rangle\,\langle\Theta|\tilde{R}_n\rangle}{\tilde{\lambda}_n} \right\rangle, \tag{44}$$

where we have introduced

$$\langle\Theta| := \left[\sum_{j\neq 1} r^y_{1j}\tilde{\mathcal{J}}^{xx}_{j1}, \sum_{j\neq 1} r^y_{1j}\tilde{\mathcal{J}}^{xy}_{j1}, \sum_{j\neq 1} r^y_{1j}\tilde{\mathcal{J}}^{x\ell}_{j1}, \ldots, \right.$$
$$\left. \times \sum_{j\neq N} r^y_{Nj}\tilde{\mathcal{J}}^{xx}_{jN}, \sum_{j\neq N} r^y_{Nj}\tilde{\mathcal{J}}^{xy}_{jN}, \sum_{j\neq N} r^y_{Nj}\tilde{\mathcal{J}}^{x\ell}_{jN} \right]. \tag{45}$$

The affine rigidity can also be expressed as

$$G_{\mathrm{A}} = \frac{1}{L^2}\langle\langle Y|\Xi\rangle\rangle, \tag{46}$$

where

$$\langle Y| := \left[r^y_{1j}, 0, 0, r^y_{2j}, 0, 0, \ldots, r^y_{Nj}, 0, 0\right]. \tag{47}$$

IV. RESULTS

In this section, we present the results of eigenvalue analysis and rigidity based on the formulation explained in the previous section. In Sec. IV A, rigidity is determined using the eigenmodes of the Jacobian. Section IV B clarifies the effects of translational and rotational motions on the DOS.

A. Theoretical evaluation of G

In this subsection, the validity of the theoretical rigidity presented in the previous section is demonstrated. For this purpose, at first, we examine the validity of Eq. (38), obtained by the eigenfunction expansion of the nonaffine displacements for the RHS and by the simulation for the LHS. Figures 3(a) and 3(b) illustrate the nonaffine displacements on the LHS and RHS of Eq. (38), respectively. In Figs. 3(a) and 3(b),

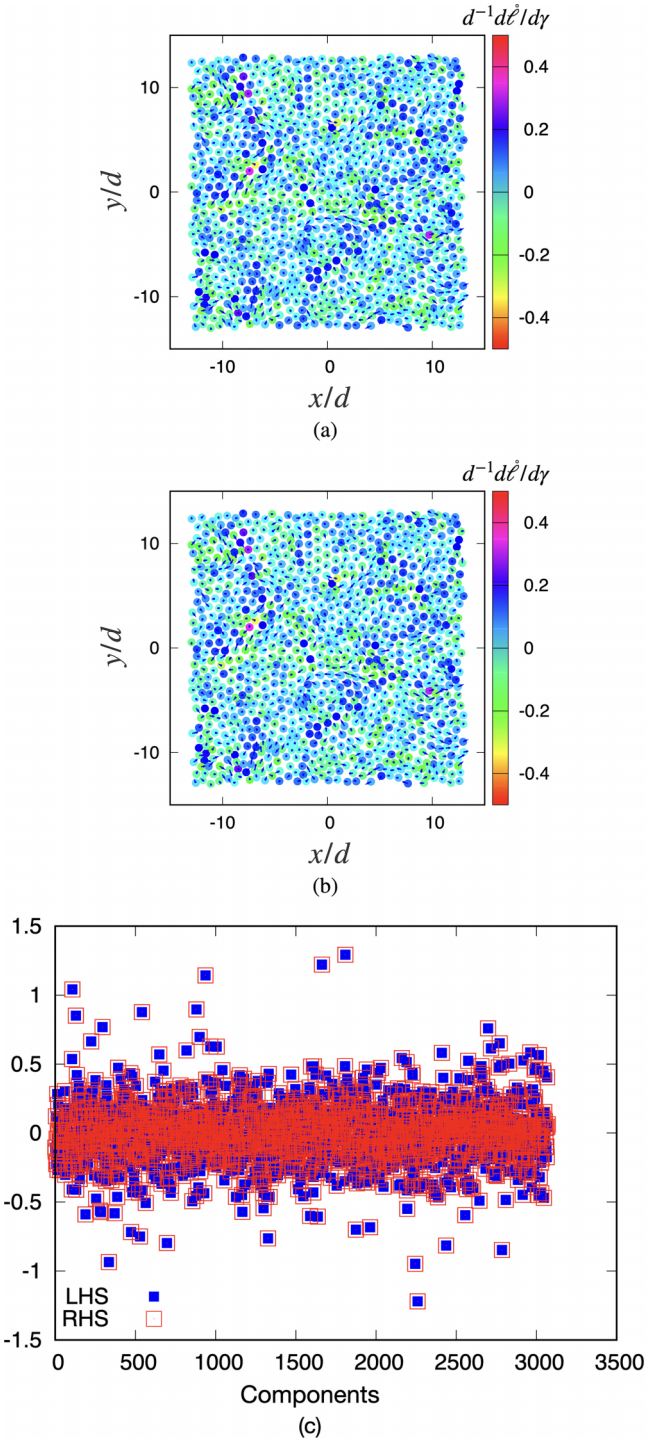

FIG. 3. Plots of nonaffine displacements on (a) the RHS of Eq. (38) obtained by eigenvalue analysis, and (b) the LHS of Eq. (38). The vector and color of each particle correspond to x, y, and ℓ components of the eigenvector of the particle, respectively. Here, the magnitude of the vectors is magnified 1.3 times for visualization. (c) Plots of the RHS (open symbols) and LHS (filled symbols) obtained by the simulation of Eq. (38) for each component whose order follows Eq. (33). These figures are based on numerical results for $N = 1024$.

(x, y) and ℓ components of $d\dot{\boldsymbol{q}}_i/d\gamma$ at $\boldsymbol{r}_i$ are represented by vectors and colors, respectively. Figure 3(c) shows the RHS and LHS of Eq. (38) against the components of the vectors whose orders follow Eq. (33), that is, the local order of the component follows x, y, and ℓ by fixing the particle number, and we align the components from the first particle to the Nth particle without omitting modes with extremely small and zero eigenvalues. Figure 3 shows that the expression in Eq. (38) correctly reproduces the simulation results.

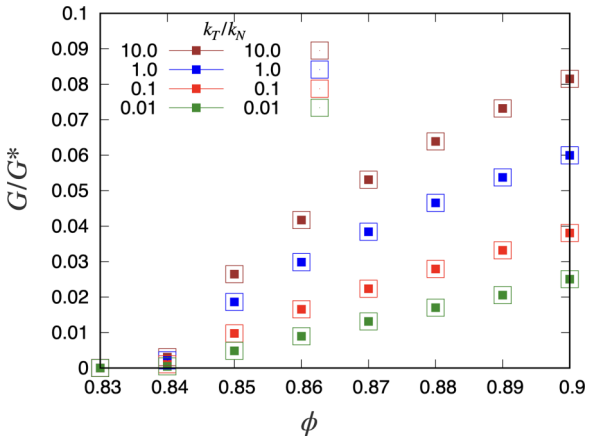

FIG. 4. Plots of theoretical [Eq. (39), open symbols] and numerical [Eq. (16), filled symbols] G against ϕ for various k_T/k_N. The figure was obtained by numerical results for $N = 1024$.

The dimensionless rigidity obtained from Eqs. (39), (40), and (44) with the aid of $G^* := k_N d^{1/2}$ is shown in Fig. 4. This indicates the quantitative agreement between the theoretical and numerical values.

Therefore, the rigidity in the linear response regime can be determined completely using the Jacobian analysis. Contrary to previous studies [6,66,67], we should note that G is not proportional to $\phi - \phi_c$ for a large k_T/k_N, where ϕ_c is the critical fraction of a jamming transition for frictional grains.

As is expected, the rigidity G depends on k_T/k_N only slightly for $k_T/k_N \leqslant 1.0 \times 10^{-4}$ (see Fig. 5), while G depends on k_T/k_N for $k_T/k_N > 10^{-4}$. We have confirmed that G smoothly approaches the frictionless value in the limit $k_T \to 0$ in contrast to Refs. [62,68]. Here, G cannot be expressed

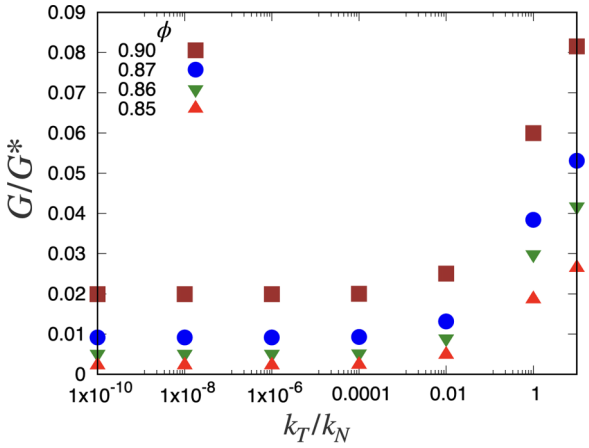

FIG. 5. Plots of numerical G against k_T/k_N for various ϕ. The figure is obtained by the numerical results for $N = 4096$.

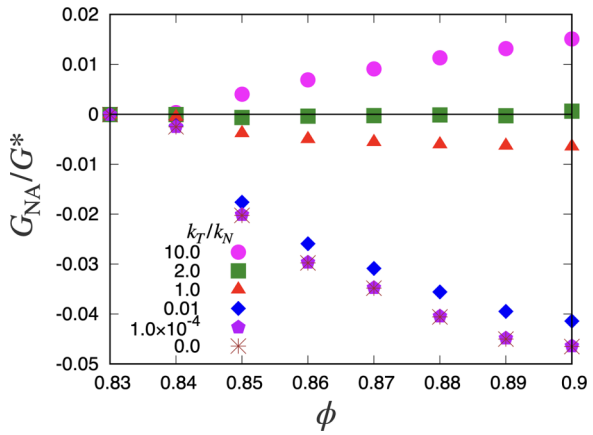

FIG. 6. Plots of G_{NA} against ϕ for various k_T/k_N. The figure is obtained by the numerical results for $N = 1024$.

as a factorization for large k_T/k_N[2]. When we consider the effect of the dynamical friction, that is, slips between particles, the rigidity is discontinuously changed in the frictionless limit [62,68]. However, the rigidity continuously changes with k_T/k_N in our system and is smoothly connected to that of frictionless systems ($k_T = 0$). Because our system can be regarded as having infinitely large static and dynamical frictional constants, there is no slip between the grains. Therefore, it might be natural for G to continuously change the limit for $k_T/k_N \to 0$ in our system. In future work, we will consider the effects of slips, which are important for real frictional grains.

To clarify the contributions of nonaffine deformations to the rigidity, we plot G_{NA} defined in Eq. (41) against ϕ in Fig. 6, in which G_{NA} becomes large as ϕ increases. Remarkably, G_{NA} is positive for $k_T/k_N > 2.0$, $G_{NA} \approx 0$ at $k_T/k_N = 2.0$, and G_{NA} is negative for $k_T/k_N < 2.0$. The positive G_{NA} for a large k_T/k_N is counterintuitive, in which G increases from G_A even when the system is relaxed to the FB state. In the future, we must clarify the origin of this counterintuitive G_{NA}. We note that the negative G_{NA} for a small k_T/k_N can be understood by the relaxation process to look for a FB configuration after applying affine deformations to the system.

B. Analysis of eigenvalues and eigenvectors

In Fig. 7 we present some typical right eigenvectors $|R_n\rangle$, which were introduced in Eq. (21) and can be expressed as

$$|R_n\rangle = \begin{bmatrix} \boldsymbol{R}_{n,1} \\ \boldsymbol{R}_{n,2} \\ \vdots \\ \boldsymbol{R}_{n,N} \end{bmatrix}, \tag{48}$$

where $\boldsymbol{R}_{n,i} := (R^x_{n,i}, R^y_{n,i}, R^\ell_{n,i})^{\mathrm{T}}$. Figure 7 illustrates vectors $(R^x_{n,i}, R^y_{n,i})^{\mathrm{T}}$ and colors to characterize the rotation $R^\ell_{n,i}$ of particle i for some characteristic ω_n with $k_T/k_N = 1.0 \times 10^{-8}$ [Figs. 7(a1)–7(a3)] and $k_T/k_N = 1.0 \times 10^{-4}$ [Figs. 7(b1)–7(b3)]. Figures 7(a1) and 7(b1) show the eigenvectors

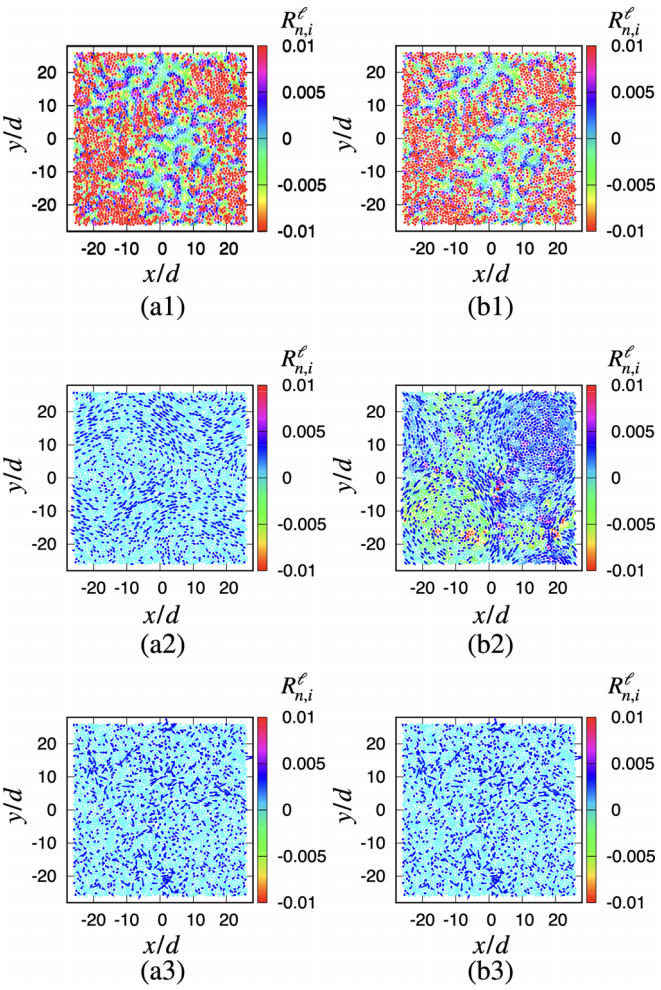

FIG. 7. Plots of eigenvectors for $\phi = 0.90$ with (a1) $\omega_n t_0 = 1.0 \times 10^{-4}$, (a2) 1.3×10^{-2}, (a3) 1.0, (b1) 1.0×10^{-2}, (b2) 1.3×10^{-2}, and (b3) 1.0, where (a1)–(a3) and (b1)–(b3) are the results for $k_T/k_N = 1.0 \times 10^{-8}$ and 1.0×10^{-4}, respectively. Here, $(R^x_{n,i}, R^y_{n,i})^{\mathrm{T}}$ and $R^\ell_{n,i}$ are represented by vectors and colors for the ith particle, respectively. Note that the magnitudes of the vectors are magnified 50 times for visualization. These figures are based on numerical results for $N = 4096$.

at $\omega_n t_0 = 1.0 \times 10^{-2}$ and $\omega_n t_0 = 1.0 \times 10^{-4}$, respectively, which are dominated by the rotational modes. In Fig. 7(a2), we confirm that the eigenvector at $\omega_n t_0 = 1.3 \times 10^{-2}$ is expressed only by translational modes, whereas the eigenvector at $\omega_n t_0 = 1.3 \times 10^{-2}$ shown in Fig. 7(b2) is expressed as a coupling mode of the rotational and translational modes. In Figs. 7(a3) and 7(b3), we show the eigenvectors at $\omega_n t_0 = 1.0$, which are dominated by the translational modes.

To clarify the translational and rotational contributions at each eigenvalue, we compute the translational and rotational participation fractions [44,46] defined as

$$\psi^T_n := \sum_{i=1}^{N} \left[\left| R^x_{n,i} \right|^2 + \left| R^y_{n,i} \right|^2 \right], \tag{49}$$

$$\psi^R_n := \sum_{i=1}^{N} \left| R^\ell_{n,i} \right|^2 = 1 - \psi^T_n, \tag{50}$$

[2]We have confirmed that the factorization $G(\phi, k_T/k_N) = G_0(\phi)\mathcal{G}(k_T/k_N)$ is not held, where $G_0(\phi)$ is the rigidity of a frictionless system.

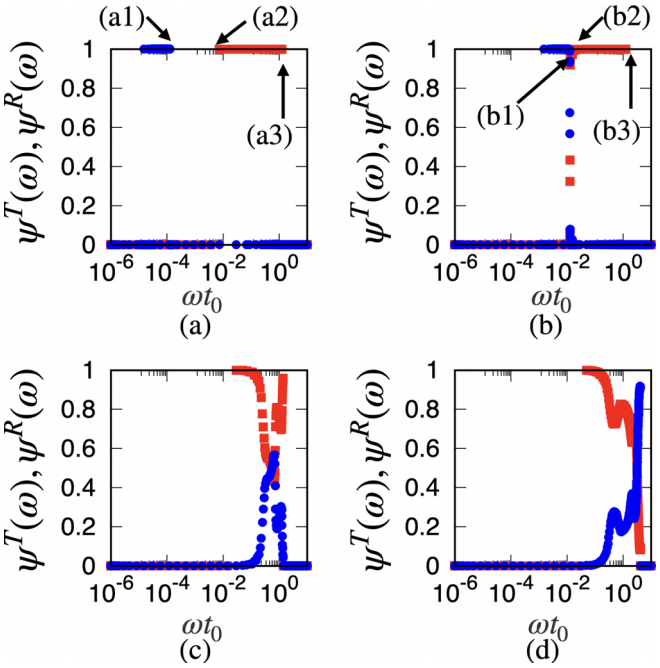

FIG. 8. Semilogarithmic plots of ψ^T (red filled squares) and ψ^R (blue filled circles) against ωt_0 for $\phi = 0.90$ at (a) $k_T/k_N = 1.0 \times 10^{-8}$, (b) 1.0×10^{-4}, (c) 1.0, and (d) 10.0. The eigenvalues of (a1), (a2), (a3), (b1), (b2), and (b3) in these figures correspond to Figs. 7(a1), 7(a2), 7(a3), 7(b1), 7(b2), and 7(b3), respectively. These figures are based on numerical results for $N = 4096$.

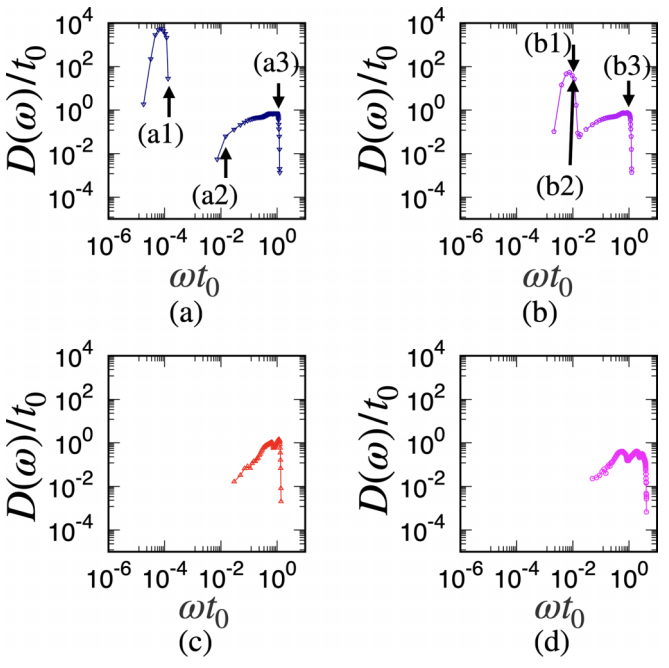

FIG. 9. Double logarithmic plots of $D(\omega)$ against ωt_0 for $\phi = 0.90$ at (a) $k_T/k_N = 1.0 \times 10^{-8}$, (b) 1.0×10^{-4}, (c) 1.0, and (d) 10.0. The eigenvalues of (a1), (a2), (a3), (b1), (b2), and (b3) in these figures correspond to Figs. 7(a1), 7(a2), 7(a3), 7(b1), 7(b2), and 7(b3), respectively. These figures are based on numerical results for $N = 4096$.

respectively, where we have investigated the localization of the system with the participation ratio in Appendix E. Note that the translational mode is dominant when ψ_n^T is close to 1, and the rotational mode is dominant when ψ_n^R is close to 1. $\psi^T(\omega)$ and $\psi^R(\omega)$ are plotted for various k_T/k_N in Fig. 8, where

$$\psi^T(\omega) := \frac{\sum_n' \langle \psi_n^T \delta(\omega - \omega_n) \rangle}{\sum_n' \langle \delta(\omega - \omega_n) \rangle}, \tag{51}$$

$$\psi^R(\omega) := \frac{\sum_n' \langle \psi_n^R \delta(\omega - \omega_n) \rangle}{\sum_n' \langle \delta(\omega - \omega_n) \rangle}. \tag{52}$$

Here, ψ^T and ψ^R are set to zero if there is no right eigenvalue for $\omega^{(s)} < \omega t_0 < \omega^{(s+1)}$ with the sth data point $\omega^{(s)}$. Here, we have used the following steps to determine each data point. First, we divided the data interval into 50 parts on a logarithmic scale. Then we linearly redivided the data interval from the highest frequency to the 10th highest frequency region. Finally, we also linearly redivided the data interval of the log scale corresponding to $0.1\sqrt{k_T/k_N} < \omega t_0 < 2\sqrt{k_T/k_N}$. Note that for the linear redivision of the data, the regions were divided into 500 or 100 equally spaced inter-regional intervals for high frequency or $0.1\sqrt{k_T/k_N} < \omega t_0 < 2\sqrt{k_T/k_N}$, respectively.

As shown in Figs. 8(a) and 8(b), we find the region of $\psi^R \simeq 1$ for low ω and $k_T/k_N < 1.0 \times 10^{-4}$. This region is referred to as Region I. We also find a region that satisfies $\psi^T \simeq 1$ for high ω and $k_T/k_N < 1.0$, in which the translational modes are dominant. This region is referred to as Region II. Here, three characteristic behaviors depend on k_T/k_N at $\phi = 0.90$. First, the translational modes are separable from the rotational modes for $k_T/k_N \leqslant 1.0 \times 10^{-8}$ because we need a small amount of energy to excite the rotational mode in nearly frictionless situations, as shown in Figs. 8(a) and 8(b). Second, the translational and rotational contributions are not separated for $1.0 \times 10^{-6} \leqslant k_T/k_N \leqslant 1.0 \times 10^{-2}$. Third, the translational and rotational contributions are indistinguishable for $k_T/k_N \geqslant 1.0$.

The DOS obtained from the Jacobian eigenvalues is shown in Fig. 9. Based on the results of $\psi^T(\omega)$ and $\psi^R(\omega)$, the DOS is also separated into two regions for $k_T/k_N \leqslant 1.0 \times 10^{-8}$. The rotational band for low ω shifts to the high ω region as k_T/k_N increases [see Figs. 9(a) and 9(b)]. In Region II with a high ω [see Figs. 9(a) and 9(b)], the DOS is almost independent of k_T/k_N, in which the translational modes are dominant for $k_T/k_N \leqslant 1.0 \times 10^{-2}$. The distinctions between the two regions for the DOS are visible with a distinct gap between the adjacent regions for $1.0 \times 10^{-10} \leqslant k_T/k_N \leqslant 1.0 \times 10^{-8}$. For $1.0 \times 10^{-6} \leqslant k_T/k_N \leqslant 1.0 \times 10^{-2}$, however, the high-$\omega$ region of the DOS in Region I partially overlaps with the low-ω region of Region II. Furthermore, Regions I and II are completely merged for $k_T/k_N \geqslant 1.0$ [see Figs. 9(c) and 9(d)]. Isolated DOS bands for low ω have been observed in systems containing anisotropic grains, such as elliptical grains and dimers [44–46]. However, to the best of our knowledge, there is no paper pointing out the existence of isolated bands of DOS in systems of frictional grains.

Because we have confirmed the existence of a peak of $D(\omega)$ around $\omega t_0 \simeq (k_T/k_N)^{1/2}$, Fig. 10 shows the scaling of the DOS in Region I by plotting $\omega_R D(\omega/\omega_R)$, where $\omega_R :=$

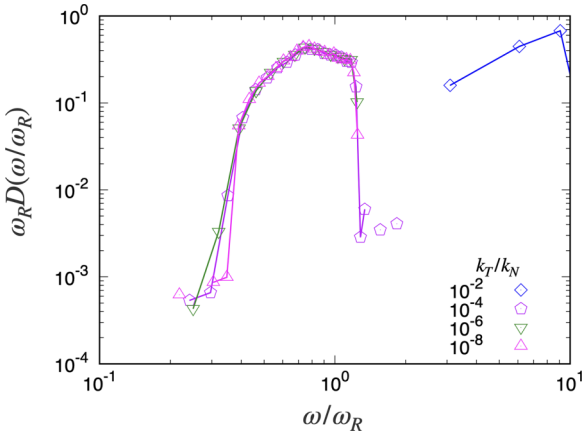

FIG. 10. Scaling plots of $\omega_R D(\omega)$ versus ω/ω_R for $\phi = 0.90$ and various k_T/k_N in $0.1 < \omega/\omega_R < 10.0$. The figure is based on numerical results for $N = 4096$.

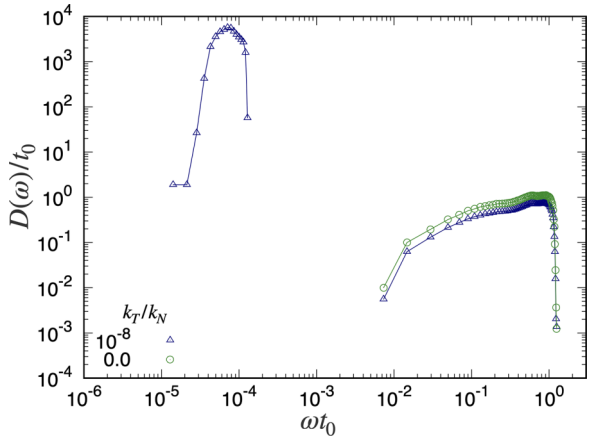

FIG. 11. Double logarithmic plots of $D(\omega)/t_0$ vs ωt_0 with $\phi = 0.90$, where red circles are the DOS for frictional grains, while blue triangles are the DOS for frictionless grains. The figure is based on numerical results for $N = 4096$.

$\sqrt{k_T/k_N}t_0^{-1}$[3]. From Fig. 10 we have confirmed that $\omega_R D(\omega)$ can be expressed as a universal scaling function of ω/ω_R for $0.1 < \omega/\omega_R < 1$ and $k_T/k_N \leqslant 0.01$.

To clarify the behavior of the DOS in the frictionless limit, we compare the DOS for $k_T/k_N = 10^{-8}$ with that for frictionless particles by plotting both cases, where we adopt the Hessian matrix to calculate the DOS for frictionless systems (see Fig. 11 and Appendix H). As expected, there is no singularity of the DOS for the translational mode, while the isolated rotational band in low ω is absent in frictionless particles, as shown in Fig. 11.

At the end of this subsection, we examine the usefulness of the effective Hessian $\mathcal{H}$ introduced in Refs. [52–54] by comparing $D(\omega)$ with $D_H(\omega)$, where $D_H(\omega)$ is the DOS obtained from $\mathcal{H}$ (see Appendix H). As shown in Figs. 12(a) and 12(b), $D(\omega)$ and $D_H(\omega)$ for various k_T/k_N are almost identical. Here, the peak of the DOS near $\omega = 0$ is caused by the rotational motion of the grains. This agreement between the Jacobian and Hessian analyses is natural because the configuration before the application of shear was prepared with frictionless particles, and the tangential displacement $\xi_{T,ij}$ is sufficiently small.

V. CONCLUDING REMARKS

We analyzed the eigenmodes of the Jacobian and obtained an expression for the rigidity of amorphous solids of frictional particles under an infinitesimal strain. We reproduced the rigidity in the linear response regime using the eigenvalues and eigenfunctions of the Jacobian with modifications in the rotational part.

Further, we confirmed that the DOS can be divided into two regions for small k_T/k_N. In the low-frequency region (Region I), the rotation of the particles plays a dominant role. These modes are characterized by the frequency $(k_T/k_N)^{1/2}/t_0$. Region I merges into the high-frequency region (Region II) for large k_T/k_N, where Region II is dominated by translational modes.

It should be noted that our results are almost independent of system size, as shown in Appendix I. Moreover, we have briefly analyzed the density dependence of the DOS in Appendix J, where the rotational band shifts to a lower frequency region, and the plateau of the translational band become longer as the density approaches the jamming point.

We have also confirmed that the results of our Jacobian analysis are almost equivalent to those of the Hessian matrix.

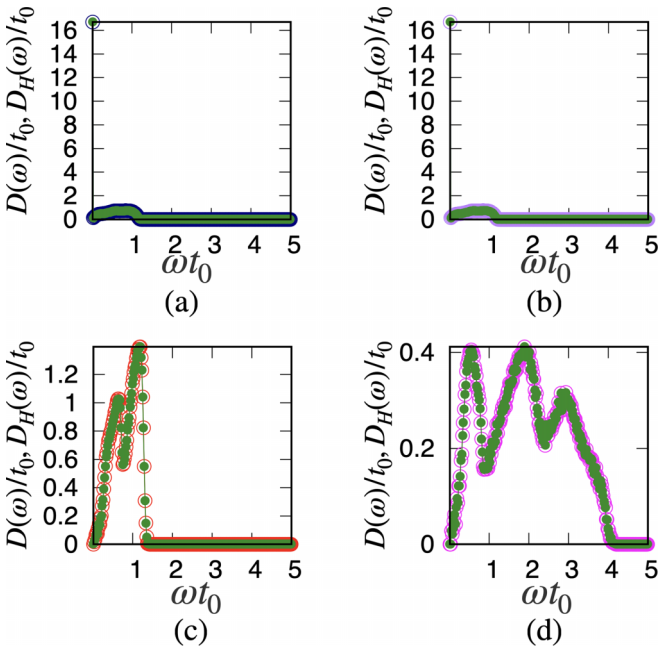

FIG. 12. Plots of $D(\omega)$ (filled symbols) and $D_H(\omega)$ (open symbols) for $\phi = 0.90$ at (a) $k_T/k_N = 1.0 \times 10^{-8}$, (b) 1.0×10^{-4}, (c) 1.0, and (d) 10.0. These figures are based on numerical results for $N = 4096$.

[3]The reason why $D(\omega)$ is multiplied by ω_R in Fig. 10 is as follows. The integral value of the DOS within Region I, $\int_{\rm I} d\omega D(\omega)$, is almost independent of k_T/k_N. Then, the LHS can be rewritten as a variable, $\int_{\rm I} d\omega D(\omega) = \int_{\rm I} d\hat{\omega} D^*(\hat{\omega})$, where $\hat{\omega} := \omega/\omega_R$, $D^*(\hat{\omega}) := \omega_R D(\omega/\omega_R)$, and $\int_{\rm I}$ represents the integral in Region I.

This is because our preparation of the initial configuration of grains is made by frictionless grains. Nevertheless, we expect that the Hessian analysis might be sufficient for stable configurations of grains.

However, the applicability of this theory is limited. The method used in this study cannot be used for finite strains because it is obvious that the eigenvectors are not orthogonal in the sheared state. Moreover, there are plastic deformations of the grains under large strains, which were not considered in this study. Therefore, we cannot predict the correct value of the theoretical rigidity at the stress drop point. More importantly, the effect of the history dependence of the frictional force is significant even in the linear response regime, although we have ignored such contacts because of the difficulty in constructing a proper theory. This issue should be addressed in future studies [71].

ACKNOWLEDGMENTS

The authors thank N. Oyama and T. Kawasaki for fruitful discussions and useful comments. This work was partially supported by a Grant-in-Aid from the MEXT for Scientific Research (Grants No. JP22K03459, No. JP21H01006, and No. JP19K03670) and by the Grant-in-Aid from the Japan Society for Promotion of Science JSPS Research Fellow (Grant No. JP20J20292).

APPENDIX A: METHOD OF PREPARING THE CONFIGURATION BEFORE APPLYING THE SHEAR

In this Appendix, we summarize the method of preparing a stable configuration of grains before applying the shear. For this purpose, as the first step, we perform the relaxation for frictionless particles with the FIRE. As the second step, the system is relaxed taking into account the static friction between particles. In the first subsection, we summarize how to prepare the configurations of frictionless particles by the FIRE [63]. In the second subsection, we describe the details of the numerical method including the force with static friction.

1. Method of preparing configuration before applying shear by FIRE

At first, we place particles at random without any overlaps of particles with the initial fraction $\phi_{\rm ini} = 0.6$. We increase the projected area fraction of the system by the increment of the fraction $\Phi := \phi^{\rm New} - \phi^{\rm Old}$ up to the target fraction ϕ, where $\phi^{\rm Old}$ and $\phi^{\rm New}$ are the projected area fraction of the system before and after each step of the increment, respectively. After each step of the increment, the system is relaxed by the FIRE [63].

To implement the process of increasing the area fraction, we scale the system as

$$L^{\rm New} = L^{\rm Old}\sqrt{\frac{\phi^{\rm Old}}{\phi^{\rm New}}}, \tag{A1}$$

$$\boldsymbol{r}_i^{\rm New} = \boldsymbol{r}_i^{\rm Old}\sqrt{\frac{\phi^{\rm Old}}{\phi^{\rm New}}}, \tag{A2}$$

where $L^{\rm Old}/L^{\rm New}$ and $\boldsymbol{r}_i^{\rm Old}/\boldsymbol{r}_i^{\rm New}$ are the linear system size and the position of the ith particle before/after rescaling, respectively. We adopt $\Phi = 10^{-4}$. When there are overlaps between particles at $\phi^{\rm New}$, the system relaxes to a stable configuration with the aid of the FIRE.

The FIRE is a fast relaxation method of minimizing potentials $U(\boldsymbol{r})$ depending on the configuration of the particles $\boldsymbol{r} := (\boldsymbol{r}_1^{\rm T}, \boldsymbol{r}_2^{\rm T}, \ldots, \boldsymbol{r}_N^{\rm T})^{\rm T}$ with $\boldsymbol{r}_i := (r_i^x, r_i^y)^{\rm T} := (x_i, y_i)^{\rm T}$ [63]. Here, we use the Hertzian potential for $U(\boldsymbol{r})$, which is defined as

$$U(\boldsymbol{r}) := \frac{2}{5}k_N \sum_{j\neq i} \xi_{N,ij}^{5/2}\Theta(d_{ij}/2 - |\boldsymbol{r}_{ij}|). \tag{A3}$$

Let us introduce the ζ-component of the force $F_{F,i}^{\zeta}$ acting on the ith particle as

$$F_{F,i}^{\zeta} := -\frac{\partial U}{\partial r_i^{\zeta}} = \sum_{j\neq i} k_N \xi_{N,ij}^{3/2} n_{ij}^{\zeta}\Theta(d_{ij}/2 - |\boldsymbol{r}_{ij}|), \tag{A4}$$

where $\zeta = x$ or y. Note that $F_{F,i}^{\zeta}$ only consists of the normal repulsive force. In the FIRE, the position $\boldsymbol{r}$ and velocity $\boldsymbol{v}_F := (\boldsymbol{v}_{F,1}, \boldsymbol{v}_{F,2}, \ldots, \boldsymbol{v}_{F,N})^{\rm T}$ with $\boldsymbol{v}_{F,i} := (v_{F,i}^x, v_{F,i}^y)^{\rm T}$ are updated by the following rules from (i) to (iv) with the variable time increment Δt_F. (i) The numerical integration via the velocity Verlet method is performed on $\boldsymbol{r}$ and $\boldsymbol{v}_F$:

$$r_i^{\zeta} \to r_i^{\zeta} + \Delta t_F v_i^{\zeta} + \Delta t_F^2 \frac{F_{F,i}^{\zeta}(\boldsymbol{r})}{2m_i}, \tag{A5}$$

$$v_{F,i}^{\zeta} \to v_{F,i}^{\zeta} + \Delta t_F \frac{F_{F,i}^{\zeta}(\tilde{\boldsymbol{r}}) + F_{F,i}^{\zeta}(\boldsymbol{r})}{2m_i}, \tag{A6}$$

where $\tilde{\boldsymbol{r}}$ is the updated configuration in Eq. (A5). (ii) We calculate $P := \boldsymbol{F}_F \cdot \boldsymbol{v}_F$, where $\boldsymbol{F}_F := (\boldsymbol{F}_{F,1}^{\rm T}, \boldsymbol{F}_{F,2}^{\rm T}, \ldots, \boldsymbol{F}_{F,N}^{\rm T})^{\rm T}$ with $\boldsymbol{F}_{F,i} := (F_{F,i}^x, F_{F,i}^y)^{\rm T}$. (iii) The velocity $\boldsymbol{v}_F$ is updated as

$$\boldsymbol{v}_{F,i} \to \boldsymbol{v}_{F,i} + \chi(\hat{\boldsymbol{v}}_{F,i} - \hat{\boldsymbol{F}}_{F,i})|\boldsymbol{v}_{F,i}|, \tag{A7}$$

where χ is the relaxation parameter, and $\hat{\boldsymbol{a}} := \boldsymbol{a}/|\boldsymbol{a}|$ for an arbitrary vector $\boldsymbol{a}$. (iv) We update χ and Δt_F in the FIRE according to the positive or negative value of P. To speed up the relaxation when the motion is along a potential gradient, we increase Δt_F. Note that this process is performed only when the number of numerical integrations along the potential gradient is larger than a certain number of times $N_{\rm min}$ to stabilize the numerical calculation. To implement this update rule, if $P > 0$ and the number of numerical integrations of $P > 0$ is larger than $N_{\rm min}$, Δt_F and χ are updated as

$$\Delta t_F \to \min(\Delta t_F f_{\rm inc}, \Delta t_{F,\rm max}), \tag{A8}$$

$$\chi \to \chi f_{\chi}, \tag{A9}$$

where $\min(a, b)$ is a selecting function of a smaller one from a and b, the parameter $f_{\rm inc}$ is introduced to speed up the relaxation, and f_{χ} and $\Delta t_{F,\rm max}$ are parameters to stabilize numerical calculations. Here, we adopt $f_{\rm inc} = 1.1$, $f_{\chi} = 0.99$, $N_{\rm min} = 5$, $\Delta t_{F,\rm max} = 10\Delta t_{F,\rm ini}$, and $\Delta t_{F,\rm ini} = 1.0 \times 10^{-2} t_0$ [63,70]. Note that $N_{\rm min}$ is necessary for the stability of the algorithm. In the case of $P \leqslant 0$, we set

$$\boldsymbol{v}_F \to \boldsymbol{0}, \tag{A10}$$

$$\chi \to \chi_{\rm start}, \tag{A11}$$

$$\Delta t_F \to \Delta t_F f_{\rm dec}, \tag{A12}$$

where we adopt $f_{\rm dec} = 0.5$ and $\chi_{\rm start} = 0.1$ [63,70].

We repeat the operations (i)–(iv) until $|F^{\zeta}_{F,i}| < F_{\rm Th}$ for arbitrary i and ζ. Note that we have used the initial values for $\Delta t_F = \Delta t_{F,\rm ini}$ and $\chi = \chi_{\rm start}$ at the starting point of the FIRE. Here, $\boldsymbol{r}$ is given and we set $\boldsymbol{v}_F = \boldsymbol{0}$ at the starting point of the FIRE.

2. Numerical method for relaxation of the configuration of frictional particles

After we obtain a stable configuration of frictionless particles at a target fraction in terms of the FIRE, we consider the effect of static friction in the relaxation process of frictional particles. The time evolution of the system is given by Eqs. (1)–(8) until $\tilde{F}^{\alpha}_i < F_{\rm Th}$ for arbitrary i and α. For the time integration, we adopt the velocity Verlet method with the time increment $\Delta t = 1.0 \times 10^{-2} t_0$.

APPENDIX B: VELOCITY VERLET METHOD IN OUR SYSTEM

In this Appendix, we first verify the accuracy of the velocity Verlet method. Next, we summarize the implementation of the velocity Verlet method. To simplify the notation, we introduce the generalized force $\tilde{\boldsymbol{f}} := (\tilde{\boldsymbol{f}}_1^{\rm T}, \tilde{\boldsymbol{f}}_2^{\rm T}, \ldots, \tilde{\boldsymbol{f}}_N^{\rm T})^{\rm T}$ with $\tilde{\boldsymbol{f}}_i := (\tilde{f}_i^x, \tilde{f}_i^y, \tilde{f}_i^{\ell})^T := (\tilde{F}_i^x/m_i^x, \tilde{F}_i^y/m_i^y, \tilde{F}_i^{\ell}/m_i^{\ell})^{\rm T}$ in this Appendix, where m_i^{α} is m_i for $\alpha = x, y$ and $4I_i/d_i^2$ for $\alpha = \ell$. Note that $\tilde{F}_i^{\alpha}$ is the generalized force, which depends on $\boldsymbol{q}$ and $\dot{\boldsymbol{q}}$ as in Eqs. (3)–(8), where $\dot{\boldsymbol{a}} := d\boldsymbol{a}/dt$ for an arbitrary vector $\boldsymbol{a}$.

1. Accuracy of the velocity Verlet method for the force depending on the velocity

In this subsection, we check the accuracy of the velocity Verlet method for the force depending on the velocity with the aid of discretization based on the Taylor expansion. The velocity Verlte method is given by a set of equations

$$q_i^{\alpha}(t+\Delta t) = q_i^{\alpha}(t) + \Delta t \dot{q}_i^{\alpha}(t) + \frac{1}{2}\Delta t^2 \tilde{f}_i^{\alpha}(t), \tag{B1}$$

$$\dot{q}_i^{\alpha}(t+\Delta t) = \dot{q}_i^{\alpha}(t) + \Delta t \frac{\tilde{f}_i^{\alpha}(t) + \tilde{f}_i^{\alpha}(t+\Delta t)}{2}. \tag{B2}$$

The first equation is called the velocity Velret equation for $q_i^{\alpha}(t)$ and the second one is the equation for $\dot{q}_i^{\alpha}(t)$. It is known that the velocity Verlet algorithm has the accuracy of $O(\Delta t^2)$ in Hamiltonian systems [69], but the accuracy of this method for dissipative dynamics is little known. Therefore, we clarify the accuracy of this method in this Appendix.

Here, we show from the Taylor expansion that the velocity Verlet method has a second-order and first-order accuracies of Δt for $\boldsymbol{q}$ and $\dot{\boldsymbol{q}}$, respectively. Based on the Taylor expansion of $q_i^{\alpha}(t+\Delta t)$, we obtain

$$\begin{aligned} q_i^{\alpha}(t+\Delta t) &= q_i^{\alpha}(t) + \Delta t \dot{q}_i^{\alpha}(t) + \tfrac{1}{2}\Delta t^2 \ddot{q}_i^{\alpha}(t) + O(\Delta t^3) \\ &= q_i^{\alpha}(t) + \Delta t \dot{q}_i^{\alpha}(t) + \tfrac{1}{2}\Delta t^2 \tilde{f}_i^{\alpha}(t) + O(\Delta t^3), \end{aligned} \tag{B3}$$

where $\dot{A} := dA/dt$ for an arbitrary function A. We can obtain the quadratic precision of Δt for $q_i^{\alpha}(t+\Delta t)$, because the RHS of Eq. (B3) is a function of current time t.

On the other hand, based on the Taylor expansion of $\dot{q}_i^{\alpha}(t+\Delta t)$, we obtain

$$\begin{aligned} \dot{q}_i^{\alpha}(t+\Delta t) &= \dot{q}_i^{\alpha}(t) + \Delta t \ddot{q}_i^{\alpha}(t) + \tfrac{1}{2}\Delta t^2 \dddot{q}_i^{\alpha}(t) + O(\Delta t^3) \\ &= \dot{q}_i^{\alpha}(t) + \Delta t \tilde{f}_i^{\alpha}(t) + \tfrac{1}{2}\Delta t^2 \dot{\tilde{f}}_i^{\alpha}(t) + O(\Delta t^3). \end{aligned} \tag{B4}$$

By using $\tilde{f}_i^{\alpha}(t+\Delta t) = \tilde{f}_i^{\alpha}(t) + \Delta t \dot{\tilde{f}}_i^{\alpha}(t) + O(\Delta t^2)$, we evaluate $\dot{\tilde{f}}_i^{\alpha}(t)$ as

$$\dot{\tilde{f}}_i^{\alpha}(t) = \frac{\tilde{f}_i^{\alpha}(t+\Delta t) - \tilde{f}_i^{\alpha}(t)}{\Delta t} + O(\Delta t). \tag{B5}$$

Substituting Eq. (B5) into Eq. (B4), we obtain [69]

$$\dot{q}_i^{\alpha}(t+\Delta t) = \dot{q}_i^{\alpha}(t) + \Delta t \frac{\tilde{f}_i^{\alpha}(t+\Delta t) + \tilde{f}_i^{\alpha}(t)}{2} + O(\Delta t^3). \tag{B6}$$

If the force $\tilde{f}_i^{\alpha}(t+\Delta t)$ is independent of $\dot{\boldsymbol{q}}$, we can obtain $\tilde{f}_i^{\alpha}(\boldsymbol{q}(t+\Delta t))$ from $\boldsymbol{q}(t+\Delta t)$ with the aid of Eq. (B3) [69]. However, if $\tilde{f}_i^{\alpha}(t+\Delta t)$ depends on $\dot{\boldsymbol{q}}$, we have to evaluate $\tilde{f}_i^{\alpha}(\boldsymbol{q}(t+\Delta t), \dot{\boldsymbol{q}}(t+\Delta t))$, because $\tilde{f}_i^{\alpha}(\boldsymbol{q}(t+\Delta t), \dot{\boldsymbol{q}}(t+\Delta t))$ requires the LHS of Eq. (B6). Thus, we adopt the following replacements:

$$\begin{aligned} \tilde{f}_i^{\alpha}(t+\Delta t) &:= \tilde{f}_i^{\alpha}(\boldsymbol{q}(t+\Delta t), \dot{\boldsymbol{q}}(t+\Delta t)) \\ &\to \tilde{f}_i^{\alpha}(\boldsymbol{q}(t+\Delta t), \dot{\boldsymbol{Q}}(t)), \end{aligned} \tag{B7}$$

$$\tilde{f}_i^{\alpha}(t) := \tilde{f}_i^{\alpha}(\boldsymbol{q}(t), \dot{\boldsymbol{q}}(t)) \to \tilde{f}_i^{\alpha}(\boldsymbol{q}(t), \dot{\boldsymbol{Q}}(t-\Delta t)), \tag{B8}$$

where we have introduced

$$\dot{Q}_i^{\alpha}(t) := \dot{q}_i^{\alpha}(t) + \Delta t \frac{\tilde{f}_i^{\alpha}(\boldsymbol{q}(t), \dot{\boldsymbol{Q}}(t-\Delta t))}{2}, \tag{B9}$$

$$\begin{aligned} \dot{Q}_i^{\alpha}(t-\Delta t) &:= \dot{q}_i^{\alpha}(t-\Delta t) \\ &\quad + \Delta t \frac{\tilde{f}_i^{\alpha}(\boldsymbol{q}(t-\Delta t), \dot{\boldsymbol{Q}}(t-2\Delta t))}{2}. \end{aligned} \tag{B10}$$

Here, the difference between $\tilde{f}_i^{\alpha}(\boldsymbol{q}(t+\Delta t), \dot{\boldsymbol{q}}(t+\Delta t))$ and $\tilde{f}_i^{\alpha}(\boldsymbol{q}(t+\Delta t), \dot{\boldsymbol{Q}}(t))$ caused by Eq. (B7) is given by

$$\begin{aligned} &\Delta \tilde{f}_i^{\alpha}(t+\Delta t) \\ &:= \tilde{f}_i^{\alpha}(\boldsymbol{q}(t+\Delta t), \dot{\boldsymbol{q}}(t+\Delta t)) - \tilde{f}_i^{\alpha}(\boldsymbol{q}(t+\Delta t), \dot{\boldsymbol{Q}}(t)) \\ &= \tilde{f}_i^{\alpha}(\boldsymbol{q}(t+\Delta t), \dot{\boldsymbol{q}}(t) + \Delta t \tilde{\boldsymbol{f}}(t) + O(\Delta t^2)) \\ &\quad - \tilde{f}_i^{\alpha}\left(\boldsymbol{q}(t+\Delta t), \dot{\boldsymbol{q}}(t) + \Delta t \frac{\tilde{\boldsymbol{f}}(\boldsymbol{q}(t), \dot{\boldsymbol{q}}(t))}{2} + O(\Delta t^2)\right) \\ &= \Delta t \sum_{j=1}^{N} \sum_{\beta = x,y,\ell} \frac{\tilde{f}_j^{\beta}(\boldsymbol{q}(t), \dot{\boldsymbol{q}}(t))}{2} \frac{\partial \tilde{f}_i^{\alpha}(\boldsymbol{q}(t), \dot{\boldsymbol{q}}(t))}{\partial \dot{q}_j^{\beta}} \\ &\quad + O(\Delta t^2). \end{aligned} \tag{B11}$$

Similarly, the difference between $\tilde{f}_i^\alpha(t) := \tilde{f}_i^\alpha(\boldsymbol{q}(t), \dot{\boldsymbol{q}}(t))$ and $\tilde{f}_i^\alpha(\boldsymbol{q}(t), \dot{\boldsymbol{Q}}(t-\Delta t))$ in Eq. (B8) can be evaluated as

$$\begin{aligned}\Delta\tilde{f}_i^\alpha(t) &:= \tilde{f}_i^\alpha(\boldsymbol{q}(t), \dot{\boldsymbol{q}}(t)) - \tilde{f}_i^\alpha(\boldsymbol{q}(t), \dot{\boldsymbol{Q}}(t-\Delta t)) \\ &= \Delta t \sum_{j=1}^{N} \sum_{\beta=x,y,\ell} \frac{\tilde{f}_j^\beta(\boldsymbol{q}(t), \dot{\boldsymbol{q}}(t))}{2} \frac{\partial \tilde{f}_i^\alpha(\boldsymbol{q}(t), \dot{\boldsymbol{q}}(t))}{\partial \dot{q}_j^\beta} \\ &\quad + O(\Delta t^2). \end{aligned} \tag{B12}$$

Thus, the replacement of Eqs. (B7) and (B8) in Eq. (B6) with Eqs. (B11) and (B12) leads to

$$\begin{aligned}&\dot{q}_i^\alpha(t+\Delta t) \\ &= \dot{q}_i^\alpha(t) + \Delta t \frac{\tilde{f}_i^\alpha(\boldsymbol{q}(t+\Delta t), \dot{\boldsymbol{Q}}(t)) + \tilde{f}(\boldsymbol{q}(t), \dot{\boldsymbol{Q}}(t-\Delta t))}{2} \\ &\quad - \Delta t^2 \sum_{j=1}^{N} \sum_{\beta=x,y,\ell} \frac{\tilde{f}_j^\beta(\boldsymbol{q}(t), \dot{\boldsymbol{q}}(t))}{2} \frac{\partial \tilde{f}_i^\alpha(\boldsymbol{q}(t), \dot{\boldsymbol{q}}(t))}{\partial \dot{q}_j^\beta} \\ &\quad + O(\Delta t^3). \end{aligned} \tag{B13}$$

Omitting the term including $O(\Delta t^2)$ in Eq. (B13), we obtain the following numerical integration methods for $\dot{\boldsymbol{q}}$:

$$\begin{aligned}&\dot{q}_i^\alpha(t+\Delta t) \to \dot{q}_i^\alpha(t) \\ &\quad + \Delta t \frac{\tilde{f}_i^\alpha(\boldsymbol{q}(t+\Delta t), \dot{\boldsymbol{Q}}(t)) + \tilde{f}(\boldsymbol{q}(t), \dot{\boldsymbol{Q}}(t-\Delta t))}{2}. \end{aligned} \tag{B14}$$

Note that Eq. (B14) is the precise expression of the velocity Verlet scheme for $\dot{\boldsymbol{q}}$ presented in Eq. (B2). From the comparison between Eqs. (B13) and (B14), we have confirmed that the velocity Verlet scheme has the first-order precision of Δt for $\dot{\boldsymbol{q}}$. We also note that if $\tilde{f}_i^\alpha$ is independent of $\dot{\boldsymbol{q}}$, as in the case of Hamiltonian systems, the term proportional to Δt^2 is zero, and thus the second-order accuracy of Δt for $\dot{q}_i^\alpha$ is guaranteed.

Let us go back to Eq. (B3) with the replacement of Eq. (B8) for $\tilde{f}_i^\alpha(t)$:

$$\begin{aligned}q_i^\alpha(t+\Delta t) &= q_i^\alpha(t) + \Delta t \dot{q}_i^\alpha(t) + \tfrac{1}{2}\Delta t^2 \tilde{f}_i^\alpha(t) + O(\Delta t^3) \\ &= q_i^\alpha(t) + \Delta t \dot{q}_i^\alpha(t) + \tfrac{1}{2}\Delta t^2 \tilde{f}_i^\alpha(\boldsymbol{q}(t), \dot{\boldsymbol{Q}}(t-\Delta t)) \\ &\quad + O(\Delta t^3). \end{aligned} \tag{B15}$$

Omitting the term including $O(\Delta t^3)$ in Eq. (B15), we obtain the following numerical integration methods for $\boldsymbol{q}$:

$$q_i^\alpha(t+\Delta t) \to q_i^\alpha(t) + \Delta t \dot{q}_i^\alpha(t) + \tfrac{1}{2}\Delta t^2 \tilde{f}_i^\alpha(\boldsymbol{q}(t), \dot{\boldsymbol{Q}}(t-\Delta t)). \tag{B16}$$

Here, Eq. (B16) is the precise expression of the velocity Verlet scheme for $\boldsymbol{q}$ presented in Eq. (B1). From Eqs. (B15) and (B16), we have confirmed that the velocity Verlet scheme has the second-order precision of Δt for $\boldsymbol{q}$.

2. Implementation of the velocity Verlet method for the force depending on the velocity

In this subsection, we explain how to adopt the velocity Verlet method in our system. In the main text, we adopt the following equations:

$$q_i^\alpha(t+\Delta t) = q_i^\alpha(t) + \Delta t \dot{q}_i^\alpha(t) + \Delta t^2 \frac{\tilde{f}_i^\alpha(\boldsymbol{q}(t), \dot{\boldsymbol{Q}}(t-\Delta t))}{2}, \tag{B17}$$

$$\dot{Q}_i^\alpha(t) = \dot{q}_i^\alpha(t) + \Delta t \frac{\tilde{f}_i^\alpha(\boldsymbol{q}(t), \dot{\boldsymbol{Q}}(t-\Delta t))}{2}. \tag{B18}$$

Here, the updated configuration $q_i^\alpha(t+\Delta t)$ and modified velocity $\dot{Q}_i^\alpha(t)$ are used to obtain the force $\tilde{f}_i^\alpha(\boldsymbol{q}(t+\Delta t), \dot{\boldsymbol{Q}}(t))$. Then, we update the velocity as follows:

$$\dot{q}_i^\alpha(t+\Delta t) = \dot{Q}_i^\alpha(t) + \Delta t \frac{\tilde{f}_i^\alpha(\boldsymbol{q}(t+\Delta t), \dot{\boldsymbol{Q}}(t))}{2}. \tag{B19}$$

APPENDIX C: JACOBIAN PROPERTIES

In this Appendix, we summarize the properties of the Jacobian introduced in Eq. (18).

1. Jacobian block elements

Let us write 3×3 submatrix $\mathcal{J}_{ij}$, which is a (ij) block element of the Jacobian obtained from Eq. (18):

$$\begin{aligned}[\mathcal{J}_{ij}]^{\alpha\beta} &:= -\frac{\partial \tilde{F}_i^\alpha}{\partial q_j^\beta} = \begin{bmatrix} -\partial_{q_j^x} F_i^x & -\partial_{q_j^y} F_i^x & -\partial_{q_j^\ell} F_i^x \\ -\partial_{q_j^x} F_i^y & -\partial_{q_j^y} F_i^y & -\partial_{q_j^\ell} F_i^y \\ -\partial_{q_j^x} \tilde{T}_i & -\partial_{q_j^y} \tilde{T}_i & -\partial_{q_j^\ell} \tilde{T}_i \end{bmatrix} = \begin{bmatrix} -\sum_{k=1;k\neq j}^N \partial_{q_j^x} f_{ik}^x & -\sum_{k=1;k\neq j}^N \partial_{q_j^y} f_{ik}^x & -\sum_{k=1;k\neq j}^N \partial_{q_j^\ell} f_{ik}^x \\ -\sum_{k=1;k\neq j}^N \partial_{q_j^x} f_{ik}^y & -\sum_{k=1;k\neq j}^N \partial_{q_j^y} f_{ik}^y & -\sum_{k=1;k\neq j}^N \partial_{q_j^\ell} f_{ik}^y \\ -\sum_{k=1;k\neq j}^N \partial_{q_j^x} \tilde{T}_{ik} & -\sum_{k=1;k\neq j}^N \partial_{q_j^y} \tilde{T}_{ik} & -\sum_{k=1;k\neq j}^N \partial_{q_j^\ell} \tilde{T}_{ik} \end{bmatrix} \\ &= \begin{cases} \begin{bmatrix} -\partial_{q_j^x} f_{ij}^x & -\partial_{q_j^y} f_{ij}^x & -\partial_{q_j^\ell} f_{ij}^x \\ -\partial_{q_j^x} f_{ij}^y & -\partial_{q_j^y} f_{ij}^y & -\partial_{q_j^\ell} f_{ij}^y \\ -\partial_{q_j^x} \tilde{T}_{ij} & -\partial_{q_j^y} \tilde{T}_{ij} & -\partial_{q_j^\ell} \tilde{T}_{ij} \end{bmatrix} (i \neq j) \\ \begin{bmatrix} -\sum_{k=1;k\neq i}^N \partial_{q_i^x} f_{ik}^x & -\sum_{k=1;k\neq i}^N \partial_{q_i^y} f_{ik}^x & -\sum_{k=1;k\neq i}^N \partial_{q_i^\ell} f_{ik}^x \\ -\sum_{k=1;k\neq i}^N \partial_{q_i^x} f_{ik}^y & -\sum_{k=1;k\neq i}^N \partial_{q_i^y} f_{ik}^y & -\sum_{k=1;k\neq i}^N \partial_{q_i^\ell} f_{ik}^y \\ -\sum_{k=1;k\neq i}^N \partial_{q_i^x} \tilde{T}_{ik} & -\sum_{k=1;k\neq i}^N \partial_{q_i^y} \tilde{T}_{ik} & -\sum_{k=1;k\neq i}^N \partial_{q_i^\ell} \tilde{T}_{ik} \end{bmatrix} (i = j) \end{cases}, \end{aligned} \tag{C1}$$

where the superscripts α and β correspond to x, y, ℓ components, and i and j are the particle numbers (see Appendix F for each component of $\mathcal{J}$). Here, f_{ij}^{ζ}, $\tilde{T}_{ij}$ are the ζ-component of $\boldsymbol{f}_{ij}$ and scaled torque that the ith particle receives from the jth particle, respectively. The submatrix for $i=j$ is given by

$$[\mathcal{J}_{ii}]^{\alpha\beta}=\begin{bmatrix}\sum_{k=1;k\neq i}^{N}\partial_{q_k^x}f_{ik}^{x} & \sum_{k=1;k\neq i}^{N}\partial_{q_k^y}f_{ik}^{x} & -\sum_{k=1;k\neq i}^{N}\partial_{q_k^\ell}f_{ik}^{x}\\ \sum_{k=1;k\neq i}^{N}\partial_{q_k^x}f_{ik}^{y} & \sum_{k=1;k\neq i}^{N}\partial_{q_k^y}f_{ik}^{y} & -\sum_{k=1;k\neq i}^{N}\partial_{q_k^\ell}f_{ik}^{y}\\ \sum_{k=1;k\neq i}^{N}\partial_{q_k^x}\tilde{T}_{ik} & \sum_{k=1;k\neq i}^{N}\partial_{q_k^y}\tilde{T}_{ik} & -\sum_{k=1;k\neq i}^{N}\partial_{q_k^\ell}\tilde{T}_{ik}\end{bmatrix}, \tag{C2}$$

where we have used $\partial_{q_i^\kappa}f_{ik}^{\zeta}=-\partial_{q_k^\kappa}f_{ik}^{\zeta}$, $\partial_{q_i^\kappa}\tilde{T}_{ik}=-\partial_{q_k^\kappa}\tilde{T}_{ik}$, $\partial_{q_i^\ell}f_{ik}^{\zeta}=\partial_{q_k^\ell}f_{ik}^{\zeta}$, and $\partial_{q_i^\ell}\tilde{T}_{ik}=\partial_{q_k^\ell}\tilde{T}_{ik}$.

Here, the superscripts ζ and κ correspond to x, y components.

From Eqs. (C1) and (C2), $\mathcal{J}_{ij}^{\zeta\beta}$ satisfies

$$\mathcal{J}_{ii}^{\zeta\beta}=-\sum_{j\neq i}\mathcal{J}_{ij}^{\zeta\beta}. \tag{C3}$$

Thus, introducing J_{nm} $(n,m=1,2,\ldots,3N)$, which is a rewriting of $\mathcal{J}_{ij}^{\alpha\beta}$ in Eq. (19) by changing the index from i and α to n, we obtain

$$\sum_{n=1,4,\ldots,3N-2}J_{nm}=0, \tag{C4}$$

$$\sum_{n=2,5,\ldots,3N-1}J_{nm}=0, \tag{C5}$$

where $\sum_{n=1,4,\ldots,3N-2}$ and $\sum_{n=2,5,\ldots,3N-1}$ express the summations of modulus 1 and modulus 2 with the intervals 3, respectively. Here, we write a $3N$-dimensional vector translating in the x direction $\boldsymbol{e}_x$ as

$$\boldsymbol{e}_x=\begin{bmatrix}\boldsymbol{e}_{x,1}\\ \boldsymbol{e}_{x,2}\\ \vdots\\ \boldsymbol{e}_{x,N}\end{bmatrix}, \tag{C6}$$

where $\boldsymbol{e}_{x,i}:=(1,0,0)^{\mathrm{T}}$ for $i=1,2,\ldots,N$. Here, the nth component of the action of $\mathcal{J}$ on $\boldsymbol{e}_x$ satisfies

$$\begin{aligned}\{\mathcal{J}\boldsymbol{e}_x\}_n&=\sum_m J_{nm}e_{x,m}\\ &=\sum_{m=1,4,\ldots,3N-2}J_{nm}\\ &=0,\end{aligned} \tag{C7}$$

where we have used Eq. (C4) for the last equality. Thus, we obtain $\mathcal{J}\boldsymbol{e}_x=\boldsymbol{0}$, where $\boldsymbol{0}$ is zero vector. Similarly, using

$$\boldsymbol{e}_y=\begin{bmatrix}\boldsymbol{e}_{y,1}\\ \boldsymbol{e}_{y,2}\\ \vdots\\ \boldsymbol{e}_{y,N}\end{bmatrix}, \tag{C8}$$

with $\boldsymbol{e}_{y,i}:=(0,1,0)^{\mathrm{T}}$, we also obtain $\mathcal{J}\boldsymbol{e}_y=\boldsymbol{0}$. Therefore, $\boldsymbol{e}_x$ and $\boldsymbol{e}_y$ are the zero modes for $\mathcal{J}$.

APPENDIX D: EXPLICIT JACOBIAN EXPRESSIONS

In this Appendix, we present the explicit expressions of the Jacobian based on Eqs. (6)–(8). Then, we clarify the difference between the present results and the case in which the tangential force is approximated by the conservative force used in the previous studies [52,53].

1. Calculation of the Jacobian

Let us consider only the normal and tangential elastic contact forces

$$\boldsymbol{f}_{N,ij}=k_N\xi_{N,ij}^{3/2}\boldsymbol{n}_{ij}, \tag{D1}$$

$$\boldsymbol{f}_{T,ij}=k_T\xi_{N,ij}^{1/2}\boldsymbol{\xi}_{T,ij}, \tag{D2}$$

where the integration of $d\boldsymbol{\xi}_{T,ij}$,

$$\boldsymbol{\xi}_{T,ij}:=\int_{C_{ij}}d\boldsymbol{\xi}_{T,ij}, \tag{D3}$$

is performed during the contact between i and j particles. Since Eq. (D3) does not contain the second term on the RHS of Eq. (9), $\boldsymbol{\xi}_{T,ij}$ may not be perpendicular to $\boldsymbol{\xi}_{N,ij}$. Nevertheless, we adopt Eq. (D3) for simplicity. Here, $d\boldsymbol{\xi}_{T,ij}$ is defined as

$$d\boldsymbol{\xi}_{T,ij}=d\boldsymbol{r}_{ij}-(d\boldsymbol{r}_{ij}\cdot\boldsymbol{n}_{ij})\boldsymbol{n}_{ij}-d\boldsymbol{\ell}_{ij}\times\boldsymbol{n}_{ij}, \tag{D4}$$

where $\boldsymbol{\ell}_{ij}$ is defined as

$$\boldsymbol{\ell}_{ij}:=\begin{bmatrix}0\\ 0\\ \ell_i+\ell_j\end{bmatrix}. \tag{D5}$$

Each component of Eq. (D4) is written as

$$d\xi_{T,ij}^{x}=dr_{ij}^{x}-(d\boldsymbol{r}_{ij}\cdot\boldsymbol{n}_{ij})n_{ij}^{x}+d\ell_{ij}n_{ij}^{y}, \tag{D6}$$

$$d\xi_{T,ij}^{y}=dr_{ij}^{y}-(d\boldsymbol{r}_{ij}\cdot\boldsymbol{n}_{ij})n_{ij}^{y}-d\ell_{ij}n_{ij}^{x}. \tag{D7}$$

The derivative of the normal force is given by

$$\partial_{r_i^\zeta}f_{N,ij}^{\kappa}=k_N\left[\delta_{\zeta\kappa}\frac{\xi_{N,ij}^{3/2}}{r_{ij}}-\left(\frac{3}{2}+\frac{\xi_{N,ij}}{r_{ij}}\right)\xi_{N,ij}^{1/2}n_{ij}^{\zeta}n_{ij}^{\kappa}\right], \tag{D8}$$

$$\partial_{\ell_i}f_{N,ij}^{\kappa}=0, \tag{D9}$$

where Kronecker's delta $\delta_{\zeta\kappa}$ satisfies $\delta_{\zeta\kappa}=1$ for $\zeta=\kappa$ and $\delta_{\zeta\kappa}=0$ otherwise. We have used

$$\frac{\partial n_{ij}^{\zeta}}{\partial r_i^{\kappa}}=\frac{1}{r_{ij}}\left(\delta_{\zeta\kappa}-n_{ij}^{\zeta}n_{ij}^{\kappa}\right), \tag{D10}$$

$$\frac{\partial r_{ij}}{\partial r_i^{\zeta}}=n_{ij}^{\zeta} \tag{D11}$$

to obtain Eq. (D8).

The derivative of the tangential force is written as

$$\partial_{r_i^\zeta} f_{T,ij}^\kappa = \tfrac{1}{2} k_T \xi_{N,ij}^{-1/2} n_{ij}^\zeta \xi_{T,ij}^\kappa - k_T \xi_{N,ij}^{1/2} \left(\delta_{\zeta\kappa} - n_{ij}^\zeta n_{ij}^\kappa\right), \quad \text{(D12)}$$

$$\partial_{\ell_i} f_{T,ij}^\kappa = -\varepsilon_\kappa k_T \xi_{N,ij}^{1/2} n_{ij}^{\nu_\kappa}, \quad \text{(D13)}$$

where ε_ζ and ν_ζ are, respectively, defined as

$$\varepsilon_\zeta := \begin{cases} 1 & (\zeta = x), \\ -1 & (\zeta = y), \end{cases} \quad \text{(D14)}$$

$$\nu_\zeta := \begin{cases} y & (\zeta = x), \\ x & (\zeta = y). \end{cases} \quad \text{(D15)}$$

Here, $\partial_{r_i^\zeta} \xi_{T,ij}^\kappa$ and $\partial_{\ell_i} \xi_{T,ij}^\kappa$ in Eqs. (D12) and (D13) satisfy

$$\frac{\partial \xi_{T,ij}^\kappa}{\partial r_i^\zeta} = \delta_{\zeta\kappa} - n_{ij}^\zeta n_{ij}^\kappa, \quad \text{(D16)}$$

$$\frac{\partial \xi_{T,ij}^\kappa}{\partial \ell_i} = \varepsilon_\kappa n_{ij}^{\nu_\kappa}. \quad \text{(D17)}$$

The derivations of Eqs. (D16) and (D17) are as follows [55]. From Eq. (D4), $d\xi_{T,ij}^\zeta$ can be written as

$$d\xi_{T,ij}^\zeta = dr_{ij}^\zeta - (d\boldsymbol{r}_{ij} \cdot \boldsymbol{n}_{ij}) n_{ij}^\zeta + (-1)^\zeta (d\ell_i + d\ell_j) n_{ij}^{\nu_\zeta}. \quad \text{(D18)}$$

Then, $d\xi_{T,ij}^x$ satisfies

$$\begin{aligned} d\xi_{T,ij}^x &= dr_{ij}^x - \sum_{\kappa=x,y} dr_{ij}^\kappa n_{ij}^\kappa n_{ij}^x + n_{ij}^y (d\ell_i + d\ell_j) \\ &= \left[1 - \left(n_{ij}^x\right)^2\right] dr_{ij}^x - n_{ij}^x n_{ij}^y dr_{ij}^y + n_{ij}^y (d\ell_i + d\ell_j) \\ &= \left(n_{ij}^y\right)^2 dr_{ij}^x - n_{ij}^x n_{ij}^y dr_{ij}^y + n_{ij}^y (d\ell_i + d\ell_j) \\ &= \left(n_{ij}^y\right)^2 (dx_i - dx_j) - n_{ij}^x n_{ij}^y (dy_i - dy_j) \\ &\quad + n_{ij}^y (d\ell_i + d\ell_j). \end{aligned} \quad \text{(D19)}$$

Similarly, $d\xi_{T,ij}^y$ also satisfies

$$\begin{aligned} d\xi_{T,ij}^y &= -n_{ij}^x n_{ij}^y (dx_i - dx_j) + \left(n_{ij}^y\right)^2 (dy_i - dy_j) \\ &\quad - n_{ij}^x (d\ell_i + d\ell_j). \end{aligned} \quad \text{(D20)}$$

Here, $d\xi_{T,ij}^\zeta$ is the function of x_i, y_i, ℓ_i, x_j, y_j, and ℓ_j. We obtain the differential form of $d\xi_{T,ij}^\zeta$:

$$\begin{aligned} d\xi_{T,ij}^\zeta &= \left(\frac{\partial \xi_{T,ij}^\zeta}{\partial x_i}\right)_{(y_i,\ell_i,x_j,y_j,\ell_j)} dx_i + \left(\frac{\partial \xi_{T,ij}^\zeta}{\partial x_j}\right)_{(x_i,y_i,\ell_i,y_j,\ell_j)} dx_j \\ &\quad + \left(\frac{\partial \xi_{T,ij}^\zeta}{\partial y_i}\right)_{(x_i,\ell_i,x_j,y_j,\ell_j)} dy_i + \left(\frac{\partial \xi_{T,ij}^\zeta}{\partial y_j}\right)_{(x_i,y_i,\ell_i,x_j,\ell_j)} dy_j \\ &\quad + \left(\frac{\partial \xi_{T,ij}^\zeta}{\partial \ell_i}\right)_{(x_i,y_i,x_j,y_j,\ell_j)} d\ell_i + \left(\frac{\partial \xi_{T,ij}^\zeta}{\partial \ell_j}\right)_{(x_i,y_i,\ell_i,x_j,y_j)} d\ell_j. \end{aligned} \quad \text{(D21)}$$

Then, we obtain Eqs. (D16) and (D17) by comparing Eqs. (D19) and (D20) with Eq. (D21).

Since the scaled torque $\tilde{T}_{ij}$ satisfies

$$\tilde{T}_{ij} := \frac{2T_{ij}}{d_i} = -n_{ij}^x f_{T,ij}^y + n_{ij}^y f_{T,ij}^x, \quad \text{(D22)}$$

we obtain

$$\begin{aligned} \partial_{r_i^\zeta} \tilde{T}_{ij} &= -\left(\partial_{r_i^\zeta} n_{ij}^x\right) f_{T,ij}^y - n_{ij}^x \partial_{r_i^\zeta} f_{T,ij}^y + \left(\partial_{r_i^\zeta} n_{ij}^y\right) f_{T,ij}^x + n_{ij}^y \partial_{r_i^\zeta} f_{T,ij}^x \\ &= -\left(\frac{\delta_{\zeta x}}{r_{ij}} - \frac{n_{ij}^\zeta n_{ij}^x}{r_{ij}}\right) f_{T,ij}^y - n_{ij}^x \left[\frac{1}{2} k_T \xi_{N,ij}^{-1/2} \xi_{T,ij} n_{ij}^\zeta t_{ij}^y - k_T \xi_{N,ij}^{1/2} \left(\delta_{\zeta y} - n_{ij}^\zeta n_{ij}^y\right)\right] \\ &\quad + \left(\frac{\delta_{\zeta y}}{r_{ij}} - \frac{n_{ij}^\zeta n_{ij}^y}{r_{ij}}\right) f_{T,ij}^x + n_{ij}^y \left[\frac{1}{2} k_T \xi_{N,ij}^{-1/2} \xi_{T,ij} n_{ij}^\zeta t_{ij}^x - k_T \xi_{N,ij}^{1/2} \left(\delta_{\zeta x} - n_{ij}^\zeta n_{ij}^x\right)\right] \\ &= -n_{ij}^x \left[\frac{1}{2} k_T \xi_{N,ij}^{-1/2} \xi_{T,ij} n_{ij}^\zeta t_{ij}^y - k_T \xi_{N,ij}^{1/2} \left(\delta_{\zeta y} - n_{ij}^\zeta n_{ij}^y\right)\right] + n_{ij}^y \left[\frac{1}{2} k_T \xi_{N,ij}^{-1/2} \xi_{T,ij} n_{ij}^\zeta t_{ij}^x - k_T \xi_{N,ij}^{1/2} \left(\delta_{\zeta x} - n_{ij}^\zeta n_{ij}^x\right)\right] \\ &= -n_{ij}^x \left[\frac{1}{2} k_T \xi_{N,ij}^{-1/2} \xi_{T,ij} n_{ij}^\zeta t_{ij}^y - k_T \xi_{N,ij}^{1/2} \delta_{\zeta y}\right] + n_{ij}^y \left[\frac{1}{2} k_T \xi_{N,ij}^{-1/2} \xi_{T,ij} n_{ij}^\zeta t_{ij}^x - k_T \xi_{N,ij}^{1/2} \delta_{\zeta x}\right], \end{aligned} \quad \text{(D23)}$$

$$\begin{aligned} \partial_{\ell_i} \tilde{T}_{ij} &= -n_{ij}^x \partial_{\ell_i} f_{T,ij}^y + n_{ij}^y \partial_{\ell_i} f_{T,ij}^x \\ &= -n_{ij}^x k_T \xi_{N,ij}^{1/2} n_{ij}^x - n_{ij}^y k_T \xi_{N,ij}^{1/2} n_{ij}^y \\ &= -k_T \xi_{N,ij}^{1/2}, \end{aligned} \quad \text{(D24)}$$

where we have used $\sum_\zeta f_{T,ij}^\zeta n_{ij}^\zeta = 0$.

The terms proportional to $\xi_{T,ij}$ in the Jacobian include the history-dependent tangential displacements, which are ignored in the effective potential (see Appendix H) [52–54]. The reason we use the Jacobian is to include the history-dependent tangential displacements in the dynamical matrix.

APPENDIX E: EFFECTS OF RATTLERS

In this Appendix, we investigate the effects of rattlers. In the first subsection, we investigate the effects of rattlers for the DOS. In the second subsection, we clarify the contributions of rattlers by using the participation ratio.

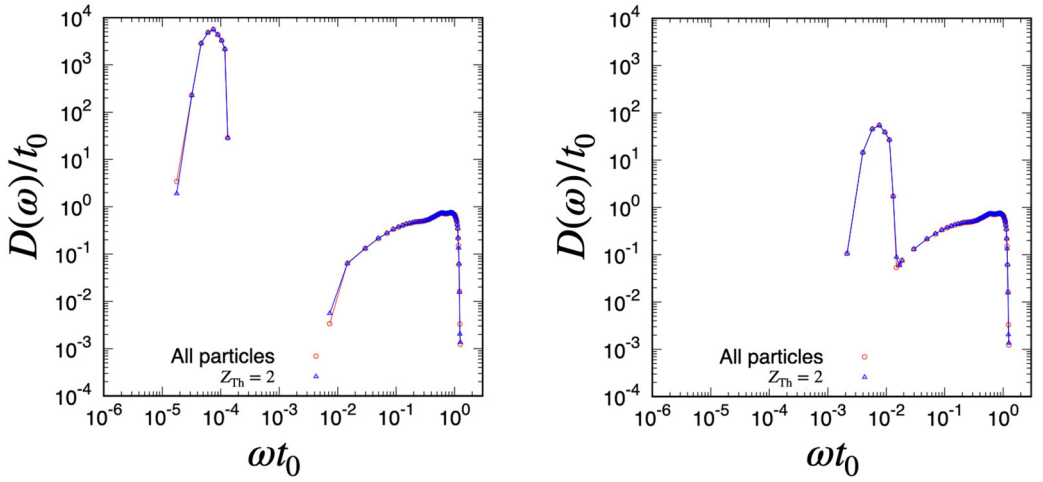

FIG. 13. Double logarithmic plots of $D(\omega)$ with (red circles) and without (blue triangles by using $Z_{\rm Th} = 2$) rattlers against ωt_0 for $\phi = 0.90$ at (a) $k_T/k_N = 1.0 \times 10^{-8}$ and (b) $k_T/k_N = 1.0 \times 10^{-4}$. These figures are based on numerical results for $N = 4096$.

1. Effects of rattlers on the DOS

In this subsection, we investigate the role of rattlers. We call particle i a rattler if its coordination number Z_i is $Z_i \leqslant Z_{\rm Th}$. Since the coordination number of the isostatic state is 3, $Z_{\rm Th}$ can be 1 or 2 for frictional grains. The rattlers are determined by the following method. Given a particle configuration, we measure the coordination number $Z_i^{(n=1)}$ of each particle. Then, we regard N_1 particles satisfying $Z_i^{(n=1)} \leqslant Z_{\rm Th}$ as rattlers at the first trial. We measure the coordination number $Z_i^{(n=2)}$ after we remove the rattler particles. In the second trial, we regard particles satisfying $Z_i^{(n=2)} \leqslant Z_{\rm Th}$ as new rattlers. We repeat these processes until the number of rattlers is converged. As shown in Fig. 13, where we adopt $Z_{\rm Th} = 2$, low-frequency modes in region I and intermediate modes between regions I and II are contributions from rattlers. Thus, we conclude that the contributions of rattlers on the DOS are not important.

2. Participation ratio

In this subsection, to clarify whether the mode at ω_n is localized or spread to the whole system, we introduce a participation ratio p_n [44,46],

$$p_n := \frac{\left(\sum_{i=1}^{N} |\boldsymbol{R}_{n,i}|^2\right)^2}{N \sum_{i=1}^{N} |\boldsymbol{R}_{n,i}|^4}. \tag{E1}$$

We plot $p(\omega)$ defined as

$$p(\omega) := \frac{\sum_n' \langle p_n \delta(\omega - \omega_n)\rangle}{\sum_n' \langle \delta(\omega - \omega_n)\rangle} \tag{E2}$$

against ωt_0 for $\phi = 0.90$ in Fig. 14. Note that $p(\omega)$ are set to be zero if there is no right eigenvalue in the region $(\omega^{(s)} < \omega < \omega^{(s+1)})$.

Figure 14 shows that the modes at $\omega t_0 \approx 10^{-5}$ in Fig. 14(a) and at $\omega t_0 \approx 10^{-3}$ in Fig. 14(b) are nearly equal to $p \approx 1/N$. Recalling that those modes consist of the rattler, we conclude that the contribution of the rattler is localized. In the middle range of ω in Fig. 14, there is an isolated band that shifts to the large ω as k_T/k_N increases while maintaining its shape, which can be seen in the main text.

APPENDIX F: EXPLICIT RESULTS OF $\mathcal{J}_N$ AND $\mathcal{J}_T$

In this Appendix, we have written down the explicit results of $\mathcal{J}_N$ and $\mathcal{J}_T$. From the results for the derivative of $\tilde{F}_i^{\alpha}$ in Appendix D, the nondiagonal block elements $\mathcal{J}_{N,ij}^{\alpha\beta}$, $\mathcal{J}_{T,ij}^{\alpha\beta}$ $(i \neq j)$ are given by

$$\mathcal{J}_{N,ij}^{xx} = k_N \frac{\xi_{ij,N}^{3/2}}{r_{ij}} - k_N \left[\frac{3}{2} + \frac{\xi_{ij,N}}{r_{ij}}\right] \xi_{ij,N}^{1/2} \left(n_{ij}^x\right)^2, \tag{F1}$$

$$\mathcal{J}_{T,ij}^{xx} - k_T \xi_{ij,N}^{1/2} \left(n_{ij}^y\right)^2 + \frac{1}{2} k_T \xi_{ij,N}^{-1/2} \xi_{ij,T} n_{ij}^x t_{ij}^x, \tag{F2}$$

$$\mathcal{J}_{N,ij}^{xy} = -k_N \left[\frac{3}{2} + \frac{\xi_{ij,N}}{r_{ij}}\right] \xi_{ij,N}^{1/2} n_{ij}^x n_{ij}^y, \tag{F3}$$

$$\mathcal{J}_{T,ij}^{xy} = k_T \xi_{ij,N}^{1/2} n_{ij}^x n_{ij}^y + \frac{1}{2} k_T \xi_{ij,N}^{-1/2} \xi_{ij,T} n_{ij}^x t_{ij}^y, \tag{F4}$$

$$\mathcal{J}_{N,ij}^{x\ell} = 0, \tag{F5}$$

$$\mathcal{J}_{T,ij}^{x\ell} = k_T \xi_{ij,N}^{1/2} n_{ij}^y + \frac{1}{2} k_T \xi_{ij,N}^{-1/2} \xi_{ij,T} n_{ij}^x \left(n_{ij}^x t_{ij}^y - n_{ij}^y t_{ij}^x\right), \tag{F6}$$

$$\mathcal{J}_{N,ij}^{yx} = -k_N \left[\frac{3}{2} + \frac{\xi_{ij,N}}{r_{ij}}\right] \xi_{ij,N}^{1/2} n_{ij}^x n_{ij}^y, \tag{F7}$$

$$\mathcal{J}_{T,ij}^{yx} = k_T \xi_{ij,N}^{1/2} n_{ij}^x n_{ij}^y + \frac{1}{2} k_T \xi_{ij,N}^{-1/2} \xi_{ij,T} n_{ij}^y t_{ij}^x, \tag{F8}$$

$$\mathcal{J}_{N,ij}^{yy} = k_N \frac{\xi_{ij,N}^{3/2}}{r_{ij}} - k_N \left[\frac{3}{2} + \frac{\xi_{ij,N}}{r_{ij}}\right] \xi_{ij,N}^{1/2} \left(n_{ij}^y\right)^2, \tag{F9}$$

$$\mathcal{J}_{T,ij}^{yy} = -k_T \xi_{ij,N}^{1/2} \left(n_{ij}^x\right)^2 + \frac{1}{2} k_T \xi_{ij,N}^{-1/2} \xi_{ij,T} n_{ij}^y t_{ij}^y, \tag{F10}$$

$$\mathcal{J}_{N,ij}^{y\ell} = 0, \tag{F11}$$

$$\mathcal{J}_{T,ij}^{y\ell} = -k_T \xi_{ij,N}^{1/2} n_{ij}^x + \frac{1}{2} k_T \xi_{ij,N}^{-1/2} \xi_{ij,T} n_{ij}^y \left(n_{ij}^x t_{ij}^y - n_{ij}^y t_{ij}^x\right), \tag{F12}$$

$$\mathcal{J}_{N,ij}^{\ell x} = 0, \tag{F13}$$

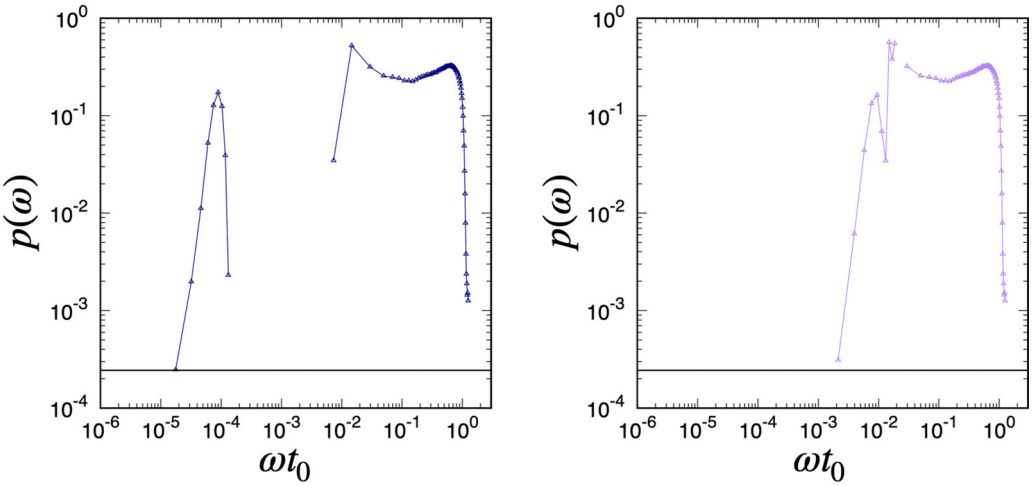

FIG. 14. Double logarithmic plots of $p(\omega)$ for $\phi = 0.90$ against ωt_0 at (a) $k_T/k_N = 1.0 \times 10^{-8}$ and (b) $k_T/k_N = 1.0 \times 10^{-4}$, where the guide line is $1/N$. These figures are based on numerical results for $N = 4096$.

$$\mathcal{J}^{\ell x}_{T,ij} = -k_T \xi^{1/2}_{ij,N} n^y_{ij}, \tag{F14}$$

$$\mathcal{J}^{\ell y}_{N,ij} = 0, \tag{F15}$$

$$\mathcal{J}^{\ell y}_{T,ij} = k_T \xi^{1/2}_{ij,N} n^x_{ij}, \tag{F16}$$

$$\mathcal{J}^{\ell \ell}_{N,ij} = 0, \tag{F17}$$

$$\mathcal{J}^{\ell \ell}_{T,ij} = k_T \xi^{1/2}_{ij,N}. \tag{F18}$$

Similarly, the diagonal block elements $\mathcal{J}^{\alpha\beta}_{N,ij}$, $\mathcal{J}^{\alpha\beta}_{T,ij}$ $(i = j)$ are given by

$$\mathcal{J}^{xx}_{N,ii} = -\sum_{j\neq i} \left\{ k_N \frac{\xi^{3/2}_{ij,N}}{r_{ij}} - k_N \left[\frac{3}{2} + \frac{\xi_{ij,N}}{r_{ij}} \right] \xi^{1/2}_{ij,N} \left(n^x_{ij}\right)^2 \right\}, \tag{F19}$$

$$\mathcal{J}^{xx}_{T,ii} = -\sum_{j\neq i} \left\{ -k_T \xi^{1/2}_{ij,N} \left(n^y_{ij}\right)^2 + \frac{1}{2} k_T \xi^{-1/2}_{ij,N} \xi_{ij,T} n^x_{ij} t^x_{ij} \right\}, \tag{F20}$$

$$\mathcal{J}^{xy}_{N,ii} = -\sum_{j\neq i} \left\{ -k_N \left[\frac{3}{2} + \frac{\xi_{ij,N}}{r_{ij}} \right] \xi^{1/2}_{ij,N} n^x_{ij} n^y_{ij} \right\}, \tag{F21}$$

$$\mathcal{J}^{xy}_{T,ii} = -\sum_{j\neq i} \left\{ k_T \xi^{1/2}_{ij,N} n^x_{ij} n^y_{ij} + \frac{1}{2} k_T \xi^{-1/2}_{ij,N} \xi_{ij,T} n^x_{ij} t^y_{ij} \right\}, \tag{F22}$$

$$\mathcal{J}^{x\ell}_{N,ii} = 0, \tag{F23}$$

$$\mathcal{J}^{x\ell}_{T,ii} = \sum_{j\neq i} \left\{ k_T \xi^{1/2}_{ij,N} n^y_{ij} + \frac{1}{2} \xi^{-1/2}_{ij,N} \xi_{ij,T} n^x_{ij} \left(n^x_{ij} t^y_{ij} - n^y_{ij} t^x_{ij} \right) \right\}, \tag{F24}$$

$$\mathcal{J}^{yx}_{N,ii} = -\sum_{j\neq i} \left\{ -k_N \left[\frac{3}{2} + \frac{\xi_{ij,N}}{r_{ij}} \right] \xi^{1/2}_{ij,N} n^x_{ij} n^y_{ij} \right\}, \tag{F25}$$

$$\mathcal{J}^{yx}_{T,ii} = -\sum_{j\neq i} \left\{ k_T \xi^{1/2}_{ij,N} n^x_{ij} n^y_{ij} + \frac{1}{2} k_T \xi^{-1/2}_{ij,N} \xi_{ij,T} n^y_{ij} t^x_{ij} \right\}, \tag{F26}$$

$$\mathcal{J}^{yy}_{N,ii} = -\sum_{j\neq i} \left\{ k_N \frac{\xi^{3/2}_{ij,N}}{r_{ij}} - k_N \left[\frac{3}{2} + \frac{\xi_{ij,N}}{r_{ij}} \right] \xi^{1/2}_{ij,N} \left(n^y_{ij}\right)^2 \right\}, \tag{F27}$$

$$\mathcal{J}^{yy}_{T,ii} = -\sum_{j\neq i} \left\{ -k_T \xi^{1/2}_{ij,N} \left(n^x_{ij}\right)^2 + \frac{1}{2} k_T \xi^{-1/2}_{ij,N} \xi_{ij,T} n^y_{ij} t^y_{ij} \right\}, \tag{F28}$$

$$\mathcal{J}^{yy}_{N,ii} = 0, \tag{F29}$$

$$\mathcal{J}^{y\ell}_{T,ii} = -\sum_{j\neq i} \left\{ k_T \xi^{1/2}_{ij,N} n^x_{ij} + \frac{1}{2} k_T \xi^{-1/2}_{ij,N} \xi_{ij,T} n^y_{ij} \left(n^x_{ij} t^y_{ij} - n^y_{ij} t^x_{ij} \right) \right\}, \tag{F30}$$

$$\mathcal{J}^{\ell x}_{N,ii} = 0, \tag{F31}$$

$$\mathcal{J}^{\ell x}_{T,ii} = \sum_{j\neq i} k_T \xi^{1/2}_{ij,N} n^y_{ij}, \tag{F32}$$

$$\mathcal{J}^{\ell y}_{N,ii} = 0, \tag{F33}$$

$$\mathcal{J}^{\ell y}_{T,ii} = -\sum_{j\neq i} k_T \xi^{1/2}_{ij,N} n^x_{ij}, \tag{F34}$$

$$\mathcal{J}^{\ell \ell}_{N,ii} = 0, \tag{F35}$$

$$\mathcal{J}^{\ell \ell}_{T,ii} = \sum_{j\neq i} k_T \xi^{1/2}_{ij,N}. \tag{F36}$$

Note that the terms proportional to $\xi_{ij,T}$ in $\mathcal{J}_T$ include the history-dependent tangential displacements, which are ignored in the effective potential [52–54].

APPENDIX G: THE DETAILED DERIVATION OF G IN THE JACOBIAN ANALYSIS

In this Appendix we derive Eq. (38), which gives the rigidity. First, nonaffine displacements are expanded in terms of eigenfunctions of the Jacobian. Next, we express the rigidity as the eigenvalues and eigenfunctions of the Jacobian. Note that we adopt the abbreviation $dA(\boldsymbol{q}^{\rm FB}(0))/d\gamma := dA(\boldsymbol{q}(\gamma))/d\gamma|_{\boldsymbol{q}(\gamma)=\boldsymbol{q}^{\rm FB}(0)}$ in this Appendix.

1. Expansion for nonaffine displacements via the eigenfunction of the Jacobian

At the FB state, $\tilde{F}^{\alpha}_i/d\gamma$ is expressed as

$$\frac{d\tilde{F}_i^\alpha}{d\gamma} = \lim_{\Delta\gamma\to 0}\frac{\tilde{F}_i^\alpha(\boldsymbol{q}^{\mathrm{FB}}(\Delta\gamma)) - \tilde{F}_i^\alpha(\boldsymbol{q}^{\mathrm{FB}}(0))}{\Delta\gamma}$$
$$= \sum_{j\neq i}\left[\frac{\partial f_{ij}^\alpha}{\partial q_i^x}y_{ij}(\boldsymbol{q}^{\mathrm{FB}}(0)) + \sum_{\zeta=x,y}\frac{\partial f_{ij}^\alpha}{\partial r_i^\zeta}\frac{d\mathring{r}_{ij}^\zeta(\boldsymbol{q}^{\mathrm{FB}}(0))}{d\gamma} + \frac{\partial f_{ij}^\alpha}{\partial \ell_i}\left(\frac{d\mathring{\ell}_i(\boldsymbol{q}^{\mathrm{FB}}(0))}{d\gamma} + \frac{d\mathring{\ell}_j(\boldsymbol{q}^{\mathrm{FB}}(0))}{d\gamma}\right)\right]. \tag{G1}$$

Using the Jacobian, we rewrite Eq. (G1) as

$$\frac{d\tilde{F}_i^\alpha}{d\gamma} = -\sum_{j\neq i}\left[\mathcal{J}_{ji}^{\alpha x}y_{ij}(\boldsymbol{q}^{\mathrm{FB}}(0)) + \sum_{\zeta=x,y}\mathcal{J}_{ji}^{\alpha\zeta}\frac{d\mathring{r}_{ij}^\zeta(\boldsymbol{q}^{\mathrm{FB}}(0))}{d\gamma} + \mathcal{J}_{ji}^{\alpha\ell}\left(\frac{d\mathring{\ell}_i(\boldsymbol{q}^{\mathrm{FB}}(0))}{d\gamma} + \frac{d\mathring{\ell}_j(\boldsymbol{q}^{\mathrm{FB}}(0))}{d\gamma}\right)\right], \tag{G2}$$

where the first and second terms on the RHS represent the contributions from the affine and nonaffine displacements, respectively. Since the affine displacements are applied to our system instantaneously as a step strain, the integral interval of tangential displacements during the affine deformation is zero. Thus, only the normal contributions in the first term on the RHS of Eq. (G2) survive in the affine displacements. Then, we rewrite $\mathcal{J}_{ij}^{\alpha\beta}$ as $\mathcal{J}_{N,ij}^{\alpha\beta}$ in Eq. (G2):

$$\frac{d\tilde{F}_i^\alpha}{d\gamma} = -\sum_{j\neq i}\left[\mathcal{J}_{N,ji}^{\alpha x}y_{ij}(\boldsymbol{q}^{\mathrm{FB}}(0)) + \sum_{\zeta=x,y}\mathcal{J}_{ji}^{\alpha\zeta}\frac{d\mathring{r}_{ij}^\zeta(\boldsymbol{q}^{\mathrm{FB}}(0))}{d\gamma} + \mathcal{J}_{ji}^{\alpha\ell}\left(\frac{d\mathring{\ell}_i(\boldsymbol{q}^{\mathrm{FB}}(0))}{d\gamma} + \frac{d\mathring{\ell}_j(\boldsymbol{q}^{\mathrm{FB}}(0))}{d\gamma}\right)\right]. \tag{G3}$$

Introducing

$$|\Xi_i\rangle := \begin{bmatrix} \sum_{j\neq i}\mathcal{J}_{N,ji}^{xx}y_{ij} \\ \sum_{j\neq i}\mathcal{J}_{N,ji}^{xy}y_{ij} \\ \sum_{j\neq i}\mathcal{J}_{N,ji}^{x\ell}y_{ij} \end{bmatrix} \tag{G4}$$

and with the aid of $d\tilde{F}_i^\alpha/d\gamma = 0$ at the FB state in Eq. (G3), we obtain

$$\Xi_i^\alpha = -\sum_{j\neq i}\left[\sum_{\zeta=x,y}\mathcal{J}_{ji}^{\alpha\zeta}\frac{d\mathring{r}_{ij}^\zeta}{d\gamma} + \mathcal{J}_{ji}^{\alpha\ell}\left(\frac{d\mathring{\ell}_i}{d\gamma} + \frac{d\mathring{\ell}_j}{d\gamma}\right)\right]. \tag{G5}$$

Since $\mathcal{J}$ satisfies $\mathcal{J}_{ii}^{\kappa\beta} = -\sum_{j\neq i}\mathcal{J}_{ji}^{\kappa\beta}$, we obtain

$$\Xi_i^\kappa = -\sum_{\zeta=x,y}\left[\left(\sum_{j\neq i}\mathcal{J}_{ji}^{\kappa\zeta}\right)\frac{d\mathring{r}_i^\zeta}{d\gamma} - \sum_{j\neq i}\mathcal{J}_{ji}^{\kappa\zeta}\frac{d\mathring{r}_j^\zeta}{d\gamma}\right] - \left[\left(\sum_{j\neq i}\mathcal{J}_{ji}^{\kappa\ell}\right)\frac{d\mathring{\ell}_i}{d\gamma} + \sum_{j\neq i}\mathcal{J}_{ji}^{\kappa\ell}\frac{d\mathring{\ell}_j}{d\gamma}\right]$$
$$= -\sum_{\zeta=x,y}\left[-\mathcal{J}_{ii}^{\kappa\zeta}\frac{d\mathring{r}_i^\zeta}{d\gamma} - \sum_{j\neq i}\mathcal{J}_{ji}^{\kappa\zeta}\frac{d\mathring{r}_j^\zeta}{d\gamma}\right] - \left[-\mathcal{J}_{ii}^{\kappa\ell}\frac{d\mathring{\ell}_i}{d\gamma} + \sum_{j\neq i}\mathcal{J}_{ji}^{\kappa\ell}\frac{d\mathring{\ell}_j}{d\gamma}\right]$$
$$= \sum_{\zeta=x,y}\sum_{j=1}^{N}\mathcal{J}_{ji}^{\kappa\zeta}\frac{d\mathring{r}_j^\zeta}{d\gamma} + \mathcal{J}_{ii}^{\kappa\ell}\frac{d\mathring{\ell}_i}{d\gamma} - \sum_{j\neq i}\mathcal{J}_{ji}^{\kappa\ell}\frac{d\mathring{\ell}_j}{d\gamma}. \tag{G6}$$

Since $\mathcal{J}$ satisfies $\mathcal{J}_{ii}^{\ell\beta} = \sum_{j\neq i}\mathcal{J}_{ji}^{\ell\beta}$, we obtain

$$\Xi_i^\ell = -\sum_{\zeta=x,y}\left[\left(\sum_{j\neq i}\mathcal{J}_{ji}^{\ell\zeta}\right)\frac{d\mathring{r}_i^\zeta}{d\gamma} - \sum_{j\neq i}\mathcal{J}_{ji}^{\ell\zeta}\frac{d\mathring{r}_j^\zeta}{d\gamma}\right] - \left[\left(\sum_{j\neq i}\mathcal{J}_{ji}^{\ell\ell}\right)\frac{d\mathring{\ell}_i}{d\gamma} + \sum_{j\neq i}\mathcal{J}_{ji}^{\ell\ell}\frac{d\mathring{\ell}_j}{d\gamma}\right]$$
$$= -\sum_{\zeta=x,y}\left[\mathcal{J}_{ii}^{\ell\zeta}\frac{d\mathring{r}_i^\zeta}{d\gamma} - \sum_{j\neq i}\mathcal{J}_{ji}^{\ell\zeta}\frac{d\mathring{r}_j^\zeta}{d\gamma}\right] + \left[\mathcal{J}_{ii}^{\ell\ell}\frac{d\mathring{\ell}_i}{d\gamma} + \sum_{j\neq i}\mathcal{J}_{ji}^{\ell\ell}\frac{d\mathring{\ell}_j}{d\gamma}\right]$$
$$= -\sum_{\zeta=x,y}\left[\mathcal{J}_{ii}^{\ell\zeta}\frac{d\mathring{r}_i^\zeta}{d\gamma} - \sum_{j\neq i}\mathcal{J}_{ji}^{\ell\zeta}\frac{d\mathring{r}_j^\zeta}{d\gamma}\right] + \sum_{j=1}^{N}\mathcal{J}_{ji}^{\ell\ell}\frac{d\mathring{\ell}_j}{d\gamma}. \tag{G7}$$

Let us introduce $\tilde{\mathcal{J}}_{ii}^{\alpha\beta}$ as

$$\tilde{\mathcal{J}}_{ii}^{\alpha\beta} := \begin{cases} -\mathcal{J}_{ii}^{\ell x} & (\alpha = \ell,\ \beta = x), \\ -\mathcal{J}_{ii}^{\ell y} & (\alpha = \ell,\ \beta = y), \\ \mathcal{J}_{ii}^{\alpha\beta} & (\text{otherwise}), \end{cases} \tag{G8}$$

and

$$\tilde{\mathcal{J}}_{ij}^{\alpha\beta} := \mathcal{J}_{ij}^{\alpha\beta}. \tag{G9}$$

Here, $\tilde{\mathcal{J}}_{ij}$ satisfies

$$\tilde{\mathcal{J}}_{ji}^{\alpha\beta} = \begin{cases} -\mathcal{J}_{ij}^{x\ell} & (\alpha = x,\ \beta = \ell), \\ -\mathcal{J}_{ij}^{y\ell} & (\alpha = y,\ \beta = \ell), \\ \mathcal{J}_{ij}^{\alpha\beta} & (\text{otherwise}). \end{cases} \tag{G10}$$

With the aid of $\tilde{\mathcal{J}}$, Eqs. (G6) and (G7) are rewritten as

$$\begin{aligned} \Xi_i^{\alpha} &= \sum_{\zeta=x,y}\sum_{j=1}^{N} \tilde{\mathcal{J}}_{ij}^{\alpha\zeta}\frac{d\mathring{r}_j^{\zeta}}{d\gamma} + \tilde{\mathcal{J}}_{ii}^{\alpha\ell}\frac{d\mathring{\ell}_i}{d\gamma} + \sum_{j\neq i}\tilde{\mathcal{J}}_{ij}^{\alpha\ell}\frac{d\mathring{\ell}_j}{d\gamma} \\ &= \sum_{\zeta=x,y}\sum_{j=1}^{N} \tilde{\mathcal{J}}_{ij}^{\alpha\zeta}\frac{d\mathring{r}_j^{\zeta}}{d\gamma} + \sum_{j=1}^{N}\tilde{\mathcal{J}}_{ij}^{\alpha\ell}\frac{d\mathring{\ell}_j}{d\gamma} \\ &= \sum_{\beta=x,y,\ell}\sum_{j=1}^{N}\tilde{\mathcal{J}}_{ij}^{\alpha\beta}\frac{d\mathring{q}_j^{\beta}}{d\gamma}, \end{aligned} \tag{G11}$$

$$\begin{aligned} \Xi_i^{\ell} &= \sum_{\zeta=x,y}\left[\mathcal{J}_{ii}^{\ell\zeta}\frac{d\mathring{r}_i^{\zeta}}{d\gamma} + \sum_{j\neq i}\mathcal{J}_{ij}^{\ell\zeta}\frac{d\mathring{r}_j^{\zeta}}{d\gamma}\right] + \sum_{j=1}^{N}\mathcal{J}_{ji}^{\ell\ell}\frac{d\mathring{\ell}_j}{d\gamma} \\ &= \sum_{\zeta=x,y}\sum_{j=1}^{N}\mathcal{J}_{ij}^{\ell\zeta}\frac{d\mathring{r}_j^{\zeta}}{d\gamma} + \sum_{j=1}^{N}\mathcal{J}_{ji}^{\ell\ell}\frac{d\mathring{\ell}_j}{d\gamma} \\ &= \sum_{\beta=x,y,\ell}\sum_{j=1}^{N}\mathcal{J}_{ij}^{\ell\beta}\frac{d\mathring{q}_j^{\beta}}{d\gamma}. \end{aligned} \tag{G12}$$

Equations (G11) and (G12) can be rewritten as

$$\Xi_i^{\alpha} = \sum_{j=1}^{N}\sum_{\beta=x,y,\ell}\tilde{\mathcal{J}}_{ij}^{\alpha\beta}\frac{d\mathring{q}_j^{\beta}}{d\gamma}. \tag{G13}$$

Furthermore, Eq. (G13) can be expressed as

$$|\Xi\rangle = \tilde{\mathcal{J}}\left|\frac{d\mathring{q}}{d\gamma}\right\rangle, \tag{G14}$$

which corresponds to Eq. (34) in the main text, where $|d\mathring{q}/d\gamma\rangle$ is introduced in Eq. (33).

Let us expand $|d\mathring{q}/d\gamma\rangle$ by the right eigenfunction $|\tilde{R}_n\rangle$ of $\tilde{\mathcal{J}}$ as

$$\left|\frac{d\mathring{q}}{d\gamma}\right\rangle = a_n\,|\tilde{R}_n\rangle\,. \tag{G15}$$

Substituting Eq. (G15) into Eq. (G14), we obtain

$$|\Xi\rangle = \tilde{\lambda}_n a_n\,|\tilde{R}_n\rangle\,. \tag{G16}$$

Multiplying $\langle\tilde{L}_m|$ by Eq. (G16) with the aid of the orthonormal relation, we obtain

$$\begin{aligned} \langle\tilde{L}_m\,|\,\Xi\rangle &= \tilde{\lambda}_n a_n \langle\tilde{L}_m\,|\,\tilde{R}_n\rangle \\ &= \tilde{\lambda}_m a_m. \end{aligned} \tag{G17}$$

Substituting this into Eq. (G15), we obtain Eq. (38).

2. The expression of G

Let us evaluate the rigidity G defined as Eq. (17). Substituting Eqs. (14) and (15) into Eq. (17), we obtain

$$G = -\left\langle \lim_{\Delta\gamma\to 0}\frac{1}{2\Delta\gamma L^2}\sum_{i,j(i\neq j)}\left[f_{ij}^{x}(\boldsymbol{q}^{\mathrm{FB}}(\Delta\gamma))r_{ij}^{y}(\boldsymbol{q}^{\mathrm{FB}}(\Delta\gamma)) - f_{ij}^{x}(\boldsymbol{q}^{\mathrm{FB}}(0))r_{ij}^{y}(\boldsymbol{q}^{\mathrm{FB}}(0))\right]\right\rangle, \tag{G18}$$

where we have adopted the symmetric expression for i and j in the summation in Eq. (G18).

Expanding $r_{ij}^{\alpha}(\boldsymbol{q}^{\mathrm{FB}}(\Delta\gamma))$ in Eq. (G18) by $\Delta\gamma$ from the zero strain state, we obtain

$$\begin{aligned} r_{ij}^{\alpha}(\boldsymbol{q}^{\mathrm{FB}}(\Delta\gamma)) &= r_i^{\alpha}(\boldsymbol{q}^{\mathrm{FB}}(\Delta\gamma)) - r_j^{\alpha}(\boldsymbol{q}^{\mathrm{FB}}(\Delta\gamma)) \\ &\simeq r_{ij}^{\alpha}(\boldsymbol{q}^{\mathrm{FB}}(0)) + \Delta\gamma\left\{\delta_{\alpha x}\big(y_i(\boldsymbol{q}^{\mathrm{FB}}(0)) - y_j(\boldsymbol{q}^{\mathrm{FB}}(0))\big) + \frac{d\mathring{r}_i^{\alpha}(\boldsymbol{q}^{\mathrm{FB}}(0))}{d\gamma} - \frac{d\mathring{r}_j^{\alpha}(\boldsymbol{q}^{\mathrm{FB}}(0))}{d\gamma}\right\} \\ &= r_{ij}^{\alpha}(\boldsymbol{q}^{\mathrm{FB}}(0)) + \Delta\gamma\left\{\delta_{\alpha x}y_{ij}(\boldsymbol{q}^{\mathrm{FB}}(0)) + \frac{d\mathring{r}_{ij}^{\alpha}(\boldsymbol{q}^{\mathrm{FB}}(0))}{d\gamma}\right\}. \end{aligned} \tag{G19}$$

Similarly, expanding $f_{ij}^{\alpha}(\Delta\gamma)$ in Eq. (G18) from the zero strain state, we obtain

$$\begin{aligned} f_{ij}^{\alpha}(\boldsymbol{q}^{\mathrm{FB}}(\Delta\gamma)) &\simeq f_{ij}^{\alpha}(\boldsymbol{q}^{\mathrm{FB}}(0)) + \sum_{k=1}^{N}\sum_{\zeta=x,y}\Delta\gamma\frac{\partial f_{ij}^{\alpha}}{\partial r_k^{\zeta}}\frac{dr_k^{\zeta}}{d\gamma} + \sum_{k=1}^{N}\Delta\gamma\frac{\partial f_{ij}^{\alpha}}{\partial \ell_k}\frac{d\ell_k}{d\gamma} \\ &= f_{ij}^{\alpha}(\boldsymbol{q}^{\mathrm{FB}}(0)) + \sum_{\zeta=x,y}\Delta\gamma\left[\frac{\partial f_{ij}^{\alpha}}{\partial r_i^{\zeta}}\left(\delta_{\zeta x}y_i(\boldsymbol{q}^{\mathrm{FB}}(0)) + \frac{d\mathring{r}_i^{\zeta}(\boldsymbol{q}^{\mathrm{FB}}(0))}{d\gamma}\right) + \frac{\partial f_{ij}^{\alpha}}{\partial r_j^{\zeta}}\left(\delta_{\zeta x}y_j(\boldsymbol{q}^{\mathrm{FB}}(0)) + \frac{d\mathring{r}_j^{\zeta}(\boldsymbol{q}^{\mathrm{FB}}(0))}{d\gamma}\right)\right] \end{aligned}$$

$$+\Delta\gamma\left[\frac{\partial f_{ij}^{\alpha}}{\partial \ell_i}\left(\delta_{\ell x} y_i(\boldsymbol{q}^{\mathrm{FB}}(0))+\frac{d\mathring{\ell}_i(\boldsymbol{q}^{\mathrm{FB}}(0))}{d\gamma}\right)+\frac{\partial f_{ij}^{\alpha}}{\partial \ell_j}\left(\delta_{\ell x} y_j(\boldsymbol{q}^{\mathrm{FB}}(0))+\frac{d\mathring{\ell}_j(\boldsymbol{q}^{\mathrm{FB}}(0))}{d\gamma}\right)\right]. \tag{G20}$$

Furthermore, using $\partial f_{ij}^{\alpha}/\partial r_j^{\zeta}=-\partial f_{ij}^{\alpha}/\partial r_i^{\zeta}$ and $\partial f_{ij}^{\alpha}/\partial \ell_j=\partial f_{ij}^{\alpha}/\partial \ell_i$, f_{ij}^{α} can be written as

$$\begin{aligned} f_{ij}^{\alpha}(\boldsymbol{q}^{\mathrm{FB}}(\Delta\gamma))=f_{ij}^{\alpha}(\boldsymbol{q}^{\mathrm{FB}}(0))&+\sum_{\zeta=x,y}\Delta\gamma\frac{\partial f_{ij}^{\alpha}}{\partial r_i^{\zeta}}\left(\delta_{\zeta x} y_{ij}(\boldsymbol{q}^{\mathrm{FB}}(0))+\frac{d\mathring{r}_{ij}^{\zeta}(\boldsymbol{q}^{\mathrm{FB}}(0))}{d\gamma}\right)\\ &+\Delta\gamma\frac{\partial f_{ij}^{\alpha}}{\partial \ell_i}\left(\frac{d\mathring{\ell}_i(\boldsymbol{q}^{\mathrm{FB}}(0))}{d\gamma}+\frac{d\mathring{\ell}_j(\boldsymbol{q}^{\mathrm{FB}}(0))}{d\gamma}\right). \end{aligned} \tag{G21}$$

Substituting Eqs. (G19) and (G21) into Eq. (G18), we obtain

$$\begin{aligned} G=-\frac{1}{2L^2}\Bigg\langle\sum_{i,j(i\neq j)}\Bigg[&f_{ij}^{x}(\boldsymbol{q}^{\mathrm{FB}}(0))\frac{d\mathring{q}_{ij}^{y}(\boldsymbol{q}^{\mathrm{FB}}(0))}{d\gamma}+\sum_{\zeta=x,y}\frac{\partial f_{ij}^{x}(\boldsymbol{q}^{\mathrm{FB}}(0))}{\partial r_i^{\zeta}}r_{ij}^{y}(\boldsymbol{q}^{\mathrm{FB}}(0))\left(\delta_{\zeta x} y_{ij}(\boldsymbol{q}^{\mathrm{FB}}(0))+\frac{d\mathring{r}_{ij}^{\zeta}(\boldsymbol{q}^{\mathrm{FB}}(0))}{d\gamma}\right)\\ &+\frac{\partial f_{ij}^{x}(\boldsymbol{q}^{\mathrm{FB}}(0))}{\partial \ell_i}r_{ij}^{y}(\boldsymbol{q}^{\mathrm{FB}}(0))\left(\frac{d\mathring{\ell}_i(\boldsymbol{q}^{\mathrm{FB}}(0))}{d\gamma}+\frac{d\mathring{\ell}_j(\boldsymbol{q}^{\mathrm{FB}}(0))}{d\gamma}\right)\Bigg]\Bigg\rangle. \end{aligned} \tag{G22}$$

Because $\sum_{i(i\neq j)} f_{ij}^{\alpha}(\boldsymbol{q}^{\mathrm{FB}}(0))=0$ at the FB state, the first term on the RHS of Eq. (G22) can be written as

$$\begin{aligned} \sum_{i,j(i\neq j)} f_{ij}^{x}(\boldsymbol{q}^{\mathrm{FB}}(0))\frac{d\mathring{q}_{ij}^{y}(\boldsymbol{q}^{\mathrm{FB}}(0))}{d\gamma}&=\sum_{i,j(i\neq j)} f_{ij}^{x}(\boldsymbol{q}^{\mathrm{FB}}(0))\left(\frac{d\mathring{q}_{i}^{y}(\boldsymbol{q}^{\mathrm{FB}}(0))}{d\gamma}-\frac{d\mathring{q}_{j}^{y}(\boldsymbol{q}^{\mathrm{FB}}(0))}{d\gamma}\right)\\ &=\sum_{j}\left(\sum_{j(j\neq i)} f_{ij}^{x}(\boldsymbol{q}^{\mathrm{FB}}(0))\right)\frac{d\mathring{q}_{i}^{y}(\boldsymbol{q}^{\mathrm{FB}}(0))}{d\gamma}-\sum_{i}\left(\sum_{i(i\neq j)} f_{ij}^{x}(\boldsymbol{q}^{\mathrm{FB}}(0))\right)\frac{d\mathring{q}_{j}^{y}(\boldsymbol{q}^{\mathrm{FB}}(0))}{d\gamma}=0. \end{aligned} \tag{G23}$$

Thus, G is expressed as

$$\begin{aligned} G=-\frac{1}{2L^2}\Bigg\langle\sum_{i,j(i\neq j)}\Bigg[&\sum_{\zeta=x,y}\frac{\partial f_{ij}^{x}(\boldsymbol{q}^{\mathrm{FB}}(0))}{\partial r_i^{\zeta}}y_{ij}(\boldsymbol{q}^{\mathrm{FB}}(0))\left(\delta_{\zeta x} y_{ij}(\boldsymbol{q}^{\mathrm{FB}}(0))+\frac{d\mathring{r}_{ij}^{\zeta}(\boldsymbol{q}^{\mathrm{FB}}(0))}{d\gamma}\right)\\ &+\frac{\partial f_{ij}^{x}(\boldsymbol{q}^{\mathrm{FB}}(0))}{\partial \ell_i}y_{ij}(\boldsymbol{q}^{\mathrm{FB}}(0))\left(\frac{d\mathring{\ell}_i(\boldsymbol{q}^{\mathrm{FB}}(0))}{d\gamma}+\frac{d\mathring{\ell}_j(\boldsymbol{q}^{\mathrm{FB}}(0))}{d\gamma}\right)\Bigg]\Bigg\rangle. \end{aligned} \tag{G24}$$

With the aid of $\mathcal{J}_{ij}^{\alpha\beta}:=-\partial_{q_j^{\beta}} f_{ij}^{\alpha}$ $(i\neq j)$, we can express G as

$$\begin{aligned} G&=\frac{1}{2L^2}\Bigg\langle\sum_{i,j(i\neq j)}\Bigg[\sum_{\zeta=x,y} y_{ij}(\boldsymbol{q}^{\mathrm{FB}}(0))\mathcal{J}_{ji}^{x\zeta}(\boldsymbol{q}^{\mathrm{FB}}(0))\left(\delta_{\zeta x} y_{ij}(\boldsymbol{q}^{\mathrm{FB}}(0))+\frac{d\mathring{r}_{ij}^{\zeta}(\boldsymbol{q}^{\mathrm{FB}}(0))}{d\gamma}\right)\\ &\quad+y_{ij}(\boldsymbol{q}^{\mathrm{FB}}(0))\mathcal{J}_{ji}^{x\ell}(\boldsymbol{q}^{\mathrm{FB}}(0))\left(\frac{d\mathring{\ell}_i(\boldsymbol{q}^{\mathrm{FB}}(0))}{d\gamma}+\frac{d\mathring{\ell}_j(\boldsymbol{q}^{\mathrm{FB}}(0))}{d\gamma}\right)\Bigg]\Bigg\rangle\\ &=\frac{1}{2L^2}\Bigg\langle\sum_{i,j(i\neq j)}\Bigg[y_{ij}^{2}(\boldsymbol{q}^{\mathrm{FB}}(0))\mathcal{J}_{ji}^{xx}(\boldsymbol{q}^{\mathrm{FB}}(0))+\sum_{\zeta=x,y} y_{ij}(\boldsymbol{q}^{\mathrm{FB}}(0))\mathcal{J}_{ji}^{x\zeta}(\boldsymbol{q}^{\mathrm{FB}}(0))\frac{d\mathring{r}_{ij}^{\zeta}(\boldsymbol{q}^{\mathrm{FB}}(0))}{d\gamma}\\ &\quad+y_{ij}(\boldsymbol{q}^{\mathrm{FB}}(0))\mathcal{J}_{ji}^{x\ell}(\boldsymbol{q}^{\mathrm{FB}}(0))\left(\frac{d\mathring{\ell}_i(\boldsymbol{q}^{\mathrm{FB}}(0))}{d\gamma}+\frac{d\mathring{\ell}_j(\boldsymbol{q}^{\mathrm{FB}}(0))}{d\gamma}\right)\Bigg]\Bigg\rangle. \end{aligned} \tag{G25}$$

Thus, with Eqs (36) and (37), we obtain Eqs. (39)–(41).

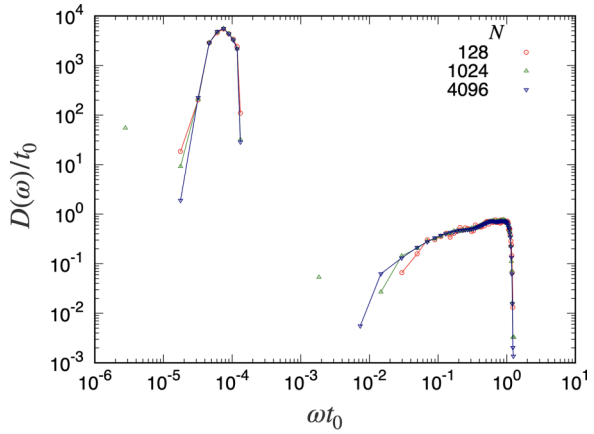

FIG. 15. Double logarithmic plots of $D(\omega)$ against ωt_0 for various N at $k_T/k_N = 1.0 \times 10^{-8}$, $\phi = 0.90$.

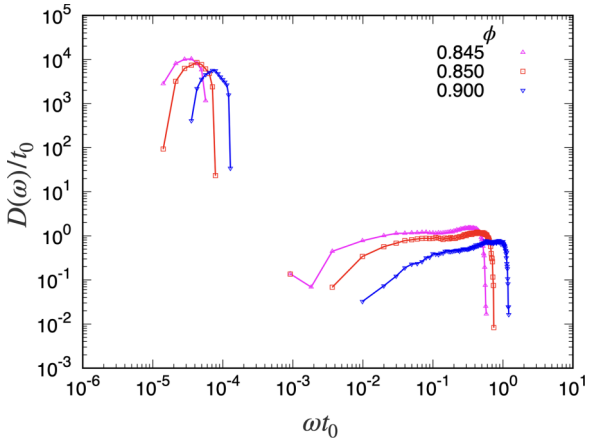

FIG. 16. Double logarithmic plots of $D(\omega)$ against ωt_0 for various ϕ at $k_T/k_N = 1.0 \times 10^{-8}$ and $N = 4096$.

APPENDIX H: DOS IN TERMS OF THE EFFECTIVE HESSIAN

In this Appendix, we introduce the DOS with the aid of the effective Hessian as in Refs. [52–54]. The effective Hessian $\mathcal{H}$ at the FB state is defined as

$$\mathcal{H}_{ij}^{\alpha\beta} := \left.\frac{\partial^2 U_{\rm eff}}{\partial q_i^\alpha \partial q_j^\beta}\right|_{\boldsymbol{q}(\gamma)=\boldsymbol{q}^{\rm FB}(0)}, \tag{H1}$$

where $U_{\rm eff}$ is the effective potential defined as

$$U_{\rm eff} := \frac{1}{2}\sum_{\langle ij\rangle}\left[k_N(\delta \boldsymbol{r}_{ij}\cdot\boldsymbol{n}_{ij})^2 - \frac{|f_{N,ij}|}{r_{ij}^{\rm FB}}(\delta \boldsymbol{r}_{ij}\cdot\boldsymbol{t}_{ij})^2 + k_T\delta t_{ij}^2\right] \tag{H2}$$

with $\delta \boldsymbol{r}_{ij} := \delta \boldsymbol{r}_i - \delta \boldsymbol{r}_j$, $\delta \boldsymbol{r}_i := \boldsymbol{r}_i - \boldsymbol{r}_i^{\rm FB}$, $r_{ij}^{\rm FB} := |\boldsymbol{r}_i^{\rm FB} - \boldsymbol{r}_j^{\rm FB}|$, $\delta t_{ij} := \delta \boldsymbol{r}_{ij}\cdot\boldsymbol{t}_{ij} - (\delta\ell_i + \delta\ell_j)$, and $\delta\ell_i := \ell_i - \ell_i^{\rm FB}$. Here, $\boldsymbol{r}_i^{\rm FB}$ and $\ell_i^{\rm FB}$ are the position of the ith particle and the third component of $\boldsymbol{q}_i$ at the FB state, respectively. Thus, $\mathcal{H}$ is a $3N \times 3N$ matrix corresponding to the Jacobian. We note that this Hessian matrix is a real symmetric matrix, and thus it can be diagonalized by an orthogonal matrix, where the eigenvectors are orthogonal with each other, and the corresponding eigenvalues are real numbers.

The eigenvalue equation of $\mathcal{H}$ is expressed as

$$\mathcal{H}\,|n\rangle = \lambda_{H,n}\,|n\rangle\,, \tag{H3}$$

where $\lambda_{H,n}$ and $|n\rangle$ are the nth eigenvalue and eigenvector of $\mathcal{H}$, respectively. Note that the left eigenvalue is also given by $\langle n|\mathcal{H} = \lambda_{H,n}\langle n|$, where $\langle n| = |n\rangle^T$. Then, we introduce the DOS D_H in terms of $\mathcal{H}$ as

$$D_H(\omega) := \frac{1}{3N}{\sum_n}'\langle\delta(\omega - \omega_{H,n})\rangle, \tag{H4}$$

where $\omega_{H,n} := \sqrt{\lambda_{H,n}}$.

APPENDIX I: SYSTEM SIZE DEPENDENCE FOR THE DOS

The system size dependence of the DOS is investigated in this Appendix. From Fig. 15 we have confirmed that both the rotational and translational bands show little dependence on system size. This means that the rotational band is not a virtual band that can only be observed in a small system, but an intrinsic band that can be observed in the thermodynamic limit. Thus, we expect that our observed results will remain unchanged even if we are interested in larger systems.

APPENDIX J: DENSITY DEPENDENCE FOR DOS

In this Appendix, we investigate the density dependence for the DOS. As shown in Fig. 16 for $k_T/k_N = 10^{-8}$, the DOS depends on ϕ, where the rotational band shifts to a lower frequency region, and the plateau of the translational band becomes longer as the density approaches the jamming point. The latter result is well known from previous studies such as Ref. [3].

[1] H. M. Jaeger, S. R. Nagel, and R. P. Behringer, Granular solids, liquids, and gases, Rev. Mod. Phys. **68**, 1259 (1996).
[2] D. J. Durian, Foam Mechanics at the Bubble Scale, Phys. Rev. Lett. **75**, 4780 (1995).
[3] M. Wyart, On the rigidity of amorphous solids, Ann. Phys. Fr. **30**, 1 (2005).
[4] A. Baule, F. Morone, H. J. Herrmann, and H. A. Makse, Edwards statistical mechanics for jammed granular matter, Rev. Mod. Phys. **90**, 015006 (2018).
[5] A. Liu and S. Nagel, Jamming is not just cool any more, Nature (London) **396**, 21 (1998).
[6] C. S. O'Hern, L. E. Silbert, A. J. Liu, and S. R. Nagel, Jamming at zero temperature and zero applied stress: The epitome of disorder, Phys. Rev. E **68**, 011306 (2003).
[7] C. S. O'Hern, S. A. Langer, A. J. Liu, and S. R. Nagel, Force Distributions near Jamming and Glass Transitions, Phys. Rev. Lett. **86**, 111 (2001).

[8] V. Trappe, V. Prasad, L. Cipelletti, P. N. Segre, and D. A. Weitz, Jamming phase diagram for attractive particles, Nature (London) **411**, 772 (2001).
[9] H. P. Zhang and H. A. Makse, Jamming transition in emulsions and granular materials, Phys. Rev. E **72**, 011301 (2005).
[10] T. S. Majmudar, M. Sperl, S. Luding, and R. P. Behringer, Jamming Transition in Granular Systems, Phys. Rev. Lett. **98**, 058001 (2007).
[11] M. P. Ciamarra, R. Pastore, M. Nicodemi, and A. Coniglio, Jamming phase diagram for frictional particles, Phys. Rev. E **84**, 041308 (2011).
[12] K. Hima Nagamanasa, S. Gokhale, A. K. Sood, and R. Ganapathy, Experimental signatures of a nonequilibrium phase transition governing the yielding of a soft glass, Phys. Rev. E **89**, 062308 (2014).
[13] E. D. Knowlton, D. J. Pine, and L. Cipelletti, A microscopic view of the yielding transition in concentrated emulsions, Soft Matter **10**, 6931 (2014).
[14] T. Kawasaki and L. Berthier, Macroscopic yielding in jammed solids is accompanied by a nonequilibrium first-order transition in particle trajectories, Phys. Rev. E **94**, 022615 (2016).
[15] P. Leishangthem, A. D. S. Parmar, and S. Sastry, The yielding transition in amorphous solids under oscillatory shear deformation, Nat. Commun. **8**, 14653 (2017).
[16] S. Dagois-Bohy, E. Somfai, B. P. Tighe, and M. van Hecke, Softening and yielding of soft glassy materials, Soft Matter **13**, 9036 (2017).
[17] M. Ozawa, L. Berthier, G. Biroli, A. Rosso, and G. Tarjus, Random critical point separates brittle and ductile yielding transitions in amorphous materials, Proc. Natl. Acad. Sci. USA **115**, 6656 (2018).
[18] A. H. Clark, J. D. Thompson, M. D. Shattuck, N. T. Ouellette, and C. S. O'Hern, Critical scaling near the yielding transition in granular media, Phys. Rev. E **97**, 062901 (2018).
[19] J. Boschan, S. Luding, and B. P. Tighe, Jamming and irreversibility, Granul. Matter **21**, 58 (2019).
[20] M. Singh, M. Ozawa, and L. Berthier, Brittle yielding of amorphous solids at finite shear rates, Phys. Rev. Mater. **4**, 025603 (2020).
[21] M. Otsuki and H. Hayakawa, Softening and Residual Loss Modulus of Jammed Grains under Oscillatory Shear in an Absorbing State, Phys. Rev. Lett. **128**, 208002 (2022).
[22] M. Wyart, S. R. Nagel, and T. A. Witten, Geometric origin of excess low-frequency vibrational modes in weakly connected amorphous solids, Europhys. Lett. **72**, 486 (2005).
[23] W. G. Ellenbroek, E. Somfai, M. van Hecke, and W. van Saarloos, Critical Scaling in Linear Response of Frictionless Granular Packings near Jamming, Phys. Rev. Lett. **97**, 258001 (2006).
[24] E. Lerner, G. Düring, and E. Bouchbinder, Statistics and Properties of Low-Frequency Vibrational Modes in Structural Glasses, Phys. Rev. Lett. **117**, 035501 (2016).
[25] L. Gartner and E. Lerner, Nonlinear plastic modes in disordered solids, Phys. Rev. E **93**, 011001(R) (2016).
[26] S. Bonfanti, R. Guerra, C. Mondal, I. Procaccia, and S. Zapperi, Elementary plastic events in amorphous silica, Phys. Rev. E **100**, 060602(R) (2019).
[27] E. DeGiuli, E. Lerner, C. Brito, and M. Wyart, Force distribution affects vibrational properties in hard-sphere glasses, Proc. Natl. Acad. Sci. USA **111**, 17054 (2014).
[28] H. Mizuno, K. Saitoh, and L. Silbert, Elastic moduli and vibrational modes in jammed particulate packings, Phys. Rev. E **93**, 062905 (2016).
[29] C. Maloney and A. Lemaître, Universal Breakdown of Elasticity at the Onset of Material Failure, Phys. Rev. Lett. **93**, 195501 (2004).
[30] C. Maloney and A. Lemaître, Amorphous systems in athermal, quasistatic shear, Phys. Rev. E **74**, 016118 (2006).
[31] A. Lemaître and C. Maloney, Sum Rules for the Quasi-Static and Visco-Elastic Response of Disordered Solids at Zero Temperature, J. Stat. Phys. **123**, 415 (2006).
[32] A. Zaccone and E. Scossa-Romano, Approximate analytical description of the nonaffine response of amorphous solids, Phys. Rev. B **83**, 184205 (2011).
[33] M. L. Manning and A. J. Liu, Vibrational Modes Identify Soft Spots in a Sheared Disordered Packing, Phys. Rev. Lett. **107**, 108302 (2011).
[34] R. Dasgupta, S. Karmakar, and I. Procaccia, Universality of the Plastic Instability in Strained Amorphous Solids, Phys. Rev. Lett. **108**, 075701 (2012).
[35] F. Ebrahem, F. Bamer, and B. Markert, Origin of reversible and irreversible atomic-scale rearrangements in a model two-dimensional network glass, Phys. Rev. E **102**, 033006 (2020).
[36] R. C. Zeller and R. O. Pohl, Thermal conductivity and specific heat of noncrystalline solids, Phys. Rev. B **4**, 2029 (1971).
[37] A. Nicolas, E. E. Ferrero, K. Martens, and J.-L. Barrat, Deformation and flow of amorphous solids: Insights from elastoplastic models, Rev. Mod. Phys. **90**, 045006 (2018).
[38] W. Schirmacher, G. Ruocco, and T. Scopigno, Acoustic Attenuation in Glasses and its Relation with the Boson Peak, Phys. Rev. Lett. **98**, 025501 (2007).
[39] H. Mizuno, H. Shiba, and A. Ikeda, Continuum limit of the vibrational properties of amorphous solids, Proc. Natl. Acad. Sci. USA **114**, 9767 (2017).
[40] L. Wang, A. Ninarello, P. Guan, L Berthier, G. Szamel, and E. Flenner, Low-frequency vibrational modes of stable glasses, Nat. Commun. **10**, 26 (2019).
[41] Z. Zeravcic, N. Xu, A. J. Liu, S. R. Nagel, and W. van Saarloos, Excitations of ellipsoid packings near jamming, Europhys. Lett. **87**, 26001 (2009).
[42] M. Mailman, C. F. Schreck, C. S. O'Hern, and B. Chakraborty, Jamming in Systems Composed of Frictionless Ellipse-Shaped Particles, Phys. Rev. Lett. **102**, 255501 (2009).
[43] C. F. Schreck, N. Xu, and C. S. O'Hern, A comparison of jamming behavior in systems composed of dimer- and ellipse-shaped particles, Soft Matter **6**, 2960 (2010).
[44] P. J. Yunker, K. Chen, Z. Zhang, W. G. Ellenbroek, A. J. Liu, and A. G. Yodh, Rotational and translational phonon modes in glasses composed of ellipsoidal particles, Phys. Rev. E **83**, 011403 (2011).
[45] C. F. Schreck, M. Mailman, B. Chakraborty, and C. S. O'Hern, Constraints and vibrations in static packings of ellipsoidal particles, Phys. Rev. E **85**, 061305 (2012).
[46] K. Shiraishi, H. Mizuno, and A. Ikeda, Vibrational properties of two-dimensional dimer packings near the jamming transition, Phys. Rev. E **100**, 012606 (2019).
[47] S. Papanikolaou, C. S. O'Hern, and M. D. Shattuck, Isostaticity at Frictional Jamming, Phys. Rev. Lett. **110**, 198002 (2013).

[48] C. Brito, H. Ikeda, P. Urbanic, M. Wyartd, and F. Zamponi, Universality of jamming of nonspherical particles, Proc. Natl. Acad. Sci. USA **115**, 11736 (2018).
[49] J. D. Treado, D. Wang, A. Boromand, M. P. Murrell, M. D. Shattuck, and C. S. O'Hern, Bridging particle deformability and collective response in soft solids, Phys. Rev. Mater. **5**, 055605 (2021).
[50] H. Ikeda, C. Brito, M. Wyart, and F. Zamponi, Jamming with Tunable Roughness, Phys. Rev. Lett. **124**, 208001 (2020).
[51] H. Ikeda, Testing mean-field theory for jamming of nonspherical particles: contact number, gap distribution, and vibrational density of states, Eur. Phys. J. E **44**, 120 (2021).
[52] E. Somfai, M. van Hecke, W. G. Ellenbroek, K. Shundyak, and W. van Saarloos, Critical and noncritical jamming of frictional grains, Phys. Rev. E **75**, 020301(R) (2007).
[53] S. Henkes, M. van Hecke, and W. van Saarloos, Critical jamming of frictional grains in the generalized isostaticity picture, Europhys. Lett. **90**, 14003 (2010).
[54] K. Liu, J. E. Kollmer, K. E. Daniels, J. M. Schwarz, and S. Henkes, Spongelike Rigid Structures in Frictional Granular Packings, Phys. Rev. Lett. **126**, 088002 (2021).
[55] J. Chattoraj, O. Gendelman, M. Pica Ciamarra, and I. Procaccia, Oscillatory Instabilities in Frictional Granular Matter, Phys. Rev. Lett. **123**, 098003 (2019).
[56] J. Chattoraj, O. Gendelman, M. P. Ciamarra, and I. Procaccia, Noise amplification in frictional systems: Oscillatory instabilities, Phys. Rev. E **100**, 042901 (2019).
[57] H. Charan, O. Gendelman, I. Procaccia, and Y. Sheffer, Giant amplification of small perturbations in frictional amorphous solids, Phys. Rev. E **101**, 062902 (2020).
[58] S. Luding, Global equation of state of two-dimensional hard sphere systems, Phys. Rev. E **63**, 042201 (2001).
[59] G. Kuwabara and K. Kono, Restitution Coefficient in a Collision between Two Spheres, Jpn. J. Appl. Phys. **26**, 1230 (1987).
[60] N. V. Brilliantov, F. Spahn, J.-M. Hertzsch, and T. Pöschel, Model for collisions in granular gases, Phys. Rev. E **53**, 5382 (1996).
[61] W. A. M. Morgado and I. Oppenheim, Energy dissipation for quasielastic granular particle collisions, Phys. Rev. E **55**, 1940 (1997).
[62] M. Otsuki and H. Hayakawa, Discontinuous change of shear modulus for frictional jammed granular materials, Phys. Rev. E **95**, 062902 (2017).
[63] E. Bitzek, P. Koskinen, F. Gähler, M. Moseler, and P. Gumbsch, Structural Relaxation Made Simple, Phys. Rev. Lett. **97**, 170201 (2006).
[64] A. Lees and S. Edwards, The computer study of transport processes under extreme conditions, J. Phys. C **5**, 1921 (1972).
[65] D. J. Evans and G. P. Morriss, *Statistical Mechanics of Nonequilibrium Liquids*, 2nd ed. (Cambridge University Press, Cambridge, UK, 2008).
[66] P. Olsson and S. Teitel, Critical scaling of shearing rheology at the jamming transition of soft-core frictionless disks, Phys. Rev. E **83**, 030302(R) (2011).
[67] M. Otsuki and H. Hayakawa, Critical scaling near jamming transition for frictional granular particles, Phys. Rev. E **83**, 051301 (2011).
[68] D. Ishima and H. Hayakawa, Scaling laws for frictional granular materials confined by constant pressure under oscillatory shear, Phys. Rev. E **101**, 042902 (2020).
[69] W. C. Swope, H. C. Andersen, P. H. Berens, and K. R. Wilson, A computer simulation method for the calculation of equilibrium constants for the formation of physical clusters of molecules: Application to small water clusters, J. Chem. Phys. **76**, 637 (1982).
[70] K. Saitoh, R. Shrivastava, and S. Luding, Rotational sound in disordered granular materials, Phys. Rev. E **99**, 012906 (2019).
[71] D. Ishima, K. Saitoh, M. Otsuki, and H. Hayakawa, Eigenvalue analysis of stress-strain curve of two-dimensional amorphous solids of dispersed frictional grains with finite shear strain, Phys. Rev. E **107**, 034904 (2023).